Transient Theory of Pumping Induced Depletion and Drawdown of a Stream with Finite Channel Storage

Bwalya Malama[1], Ying-Fan Lin[2], Hwa-Lung Yu[2], Hua-Ting Tseng[2], and Sam Greene[1]

[1]Natural Resources Management and Environmental Sciences, California Polytechnic State University, San Luis Obispo, State of California, USA

[2]Department of Bioenvironmental Systems Engineering, National Taiwan University, Taipei City, Taiwan

Correspondence: Bwalya Malama (bmalama@calpoly.edu)

Abstract. Mathematical models for stream depletion with stream stage decline or drawdown are developed to overcome the deficiency in existing models that typically use the constant-head (Dirichlet) or general (Robin) boundary condition and source terms at the stream-aquifer interface. Existing approaches assume a fixed stream stage during pumping, implies that the stream is an infinite water source, with depletion defined as a decrease in stream discharge. We refer to this depletion without draw-

5   down as the "stream depletion paradox." It is a glaring model limitation, ignoring the most observable adverse effect of long-term groundwater abstraction near a stream, namely stage declines that eventually lead to dry streambeds. Field data are presented to demonstrate that stream stage responds to pumping near the stream, motivating the development of an alternative theory predicts transient stream drawdown based on the concepts of finite stream storage and mass continuity at the stream-aquifer interface. Based on this alternative theory, models are developed for the cases of a non- and a fully-penetrating stream.

10   The proposed model reduces to the fixed-stage model in the limit as stream storage becomes infinitely large and to the limiting case of confined aquifer flow with a no-flow boundary at the streambed when the stream storage vanishes. The model is applied to field observations of both aquifer and stream drawdown from tests conducted in a confined aquifer over which a shallow stream flows. Model fits and parameter estimates are obtained both aquifer and stream drawdown data. Model-predicted and observed transient drawdown behavior indicate that fixed-stage models (a) underestimate late-time aquifer drawdown and

15   (b) overestimate the available recharge from streams to pumping wells. This has significant implications for the sustainable management of water resources in hydraulically connected stream-aquifer systems with heavy groundwater abstraction.

1   Introduction

Groundwater pumping in basins bounded by streams can lead to reduced stream flows, with undesirable impacts on both human use and ecosystem function (Winter et al., 1998; Bowen et al., 2007; Yu and Chu, 2010; Foglia et al., 2013; Zipper

20   et al., 2018; Tolley et al., 2019; Kwon et al., 2020) due to dry streambeds and disconnected stream-groundwater systems. Theis

(1941) was among the first to develop a model for stream depletion resulting from groundwater pumping from a confined aquifer. Theis (1941) used an earlier model (Theis, 1935) for a laterally infinite aquifer and the linear superposition principle to simulate a constant-head (Dirichlet) boundary condition at the stream-aquifer interface. Glover and Balmer (1954) extended upon this work with a closed-form function of the model, later tabulated by Jenkins (1968). Hantush (1965) made the next

25 notable advancement by introducing a semiprevious streambed with a general (Robin) boundary condition at the stream-aquifer interface. The Robin boundary condition implies that the flux is proportional to the differential head across the streambed, with stream stage held constant. Intaraprasong and Zhan (2009) expanded upon this work, solving the full groundwater flow equation throughout the streambed with stream stage prescribed as a time-dependent function. Chan (1976) and Asadi-Aghbolaghi and Seyyedian (2010) generalized application of the superposition principle to confined aquifer flow domains bounded laterally

30 by intersecting streams. Workers such as Grigoryev (1957), Bochever (1966), Zlotnik et al. (1999), Hunt (1999), Butler Jr et al. (2001), Fox et al. (2002), Butler Jr et al. (2007) and Zlotnik and Tartakovsky (2008) extended analytical stream depletion models to cases of partially penetrating streams. Stream depletion models where the aquifer is unconfined have been developed by Hunt (2003, 2009), who also uses a fixed-stage condition.

Numerical models, such as MODFLOW (Harbaugh, 2005) and MIKE SHE (Refsgaard et al., 2010), through their respec-

35 tive stream packages, treat stream BCs and source/drainage terms in a manner similar to the analytical models discussed above. They also allow one to specify the spatially variable stream stage using empirical hydrographs (Harbaugh, 2005) or formulas such as the Manning equation (Prudic et al., 2004). The approach is highly nonlinear, requiring iterative methods at every time step, which is computationally taxing. A comprehensive review of the literature on different configurations of pumping-induced stream depletion problems has been provided by Huang et al. (2018), where the Dirichlet and Robin boundary conditions are

40 identified as the only ones used for such problems. Where source terms are introduced in partially-penetrating stream scenarios, they are a linear function of the differential head across the streambed with a fixed stage.

As mentioned already, the models discussed above use either a constant-head or Robin boundary condition (or source term) at the stream-aquifer interface, both of which require fixed (or more generally, prescribed) stream stages with the stream acting as an indefinite source of groundwater recharge. However, streams can only provide a limited amount of water and for a

45 limited period to pumping wells. This has been recognized by others, including Zlotnik (2004), who subsequently introduced the concept of maximum stream depletion rate (SDR). As noted by Kollet and Zlotnik (2003), stream stage response to aquifer pumping can be ignored because the stream flow rate is two orders or more higher than the pumping rate. This suggests that new models that consider the stream stage drawdown response are required when the stream flow rate is small or comparable to the pumping rate. Given the limitations of the stream depletion models reviewed above, an alternative theory is proposed

50 here where a new boundary condition is imposed at the stream-aquifer interface by invoking the mass-balance principle and introducing the concept of finite stream channel storage.

Two semi-analytical solutions are developed for the cases of non- (or minimally-) penetrating (NPS) and fully-penetrating streams (FPS) in a confined aquifer. The solutions are validated by comparing them with a numerical model based on the finite-element method (FEM) as well as field observations of aquifer and stream drawdown. Li et al. (2022) proposed analytical

55 depletion functions (ADFs), to combine the advantages of analytical and numerical solutions for estimating the pumping-

induced stream depletion. The ADFs approach was tested on several existing stream depletion solutions Theis (1941); Hunt (1999) coupled with the superposition principle to estimate SDR from streamflow networks. Due to the linearity of the model proposed in the present work, it is possible to couple it with the ADFs approach to better estimate the SDR due to pumpage. Additionally, Huang et al. (2020); Xiong et al. (2021) proposed a Robin-type streambed boundary condition using the lagging

60 theory of Lin and Yeh (2017) to reflect the effect of the streambed storage. They revealed that streambed storage has a profound impact on aquifer drawdown, particularly at early times. In this work, we neglect both the ADF approach and streambed storage to focus entirely on the effect of stream channel storage and to limit the number of confounding free parameters in the mathematical model.

In the following, we describe the mathematical formulation and the proposed new boundary condition, develop semi-

65 analytical solutions for the two cases already mentioned above, validate these solutions by comparison to a finite element solution, and apply the model to field observations of stream and aquifer drawdown.

2   Mathematical Formulation

In the following, we test the hypothesis that the stream has finite storage and, using a mass conservation condition at the stream-aquifer interface, derive two solutions that allow stream stage to respond to pumping. To accomplish this, we consider

70 flow to a fully-penetrating well in a confined aquifer in the neighborhood of (a) a non-penetrating stream (NPS) and (b) a fully-penetrating stream (FPS). For the FPS, we consider two cases, namely, the case where flow in the aquifer on both sides of the stream is considered, and the case where only flow in the aquifer on the bank-side with the pumping well is considered. We assume that groundwater is pumped at a constant rate, Q [L³T⁻¹], from a line-sink located at a distance of R [L] from the stream bank. The aquifer is of infinite lateral extent away from the stream with uniform thickness b [L], and is anisotropic

75 in the horizontal (x, y) plane with the hydraulic conductivities K_x and K_y [LT⁻¹] in x- and y-directions, respectively. The aquifer interacts with the stream across a streambed with hydraulic conductivity K' [LT⁻¹] and thickness b' [L] (conductance $\beta = K'/b'$) as in Hantush (1965). The effects of streambed storage are neglected entirely with a focus only on the effects of stream channel storage. Stream stage, $H_r(t)$ [L], here is relative to the bottom of the aquifer. Stream drawdown is defined as $s_r(t) = H_0 - H_r(t)$, where H_0 [L] is the initial stream stage. The conceptual models of the problem described here are shown

80 schematically in Figure 1.

2.1   Governing Equations of Flow

The governing equation of flow problem considered in this work is (Fox et al., 2002)

$$S_s \frac{\partial s}{\partial t} = \mathbf{K} \nabla^2 s + f(x, y, t), \tag{1}$$

where $s = s(x, y, t)$ is aquifer drawdown, (x, y) are spatial coordinates in the horizontal plane, t is the elapsed time from the

85 onset of pumping, $\mathbf{K}$ is the diagonal aquifer hydraulic conductivity tensor with principal values K_x and K_y, S_s is aquifer specific storage, and $f(x, y, t)$ is a sink/source function. The x coordinate axis is perpendicular to the stream bank with the

origin on the stream bank closest to the pumping well. The y-axis is parallel to the stream channel axis and extends from $y = -\infty$ to $y = \infty$.

2.2 Non-penetrating Stream

90 We first consider the case of a stream that flows atop an aquifer to simulate the case where the stream only minimally penetrates the aquifer. We refer to this case as that of a non-penetrating stream (NPS). To solve the flow problem, aquifer drawdown is defined in a piecewise manner as

$$
s(x,y,t) = \begin{cases} s_1(x,y,t) & x > 0 \\ s_2(x,y,t) & x \in [-W,0] \\ s_3(x,y,t) & x < -W \end{cases} \tag{2}
$$

where W is the width of the stream. Also, the sink/source function, $f(x,y,t)$, is defined as

95 $$
f(x,y,t) = \frac{1}{b} \begin{cases} -Q\delta(x-R)\delta(y)/\pi & x > 0 \\ \Gamma & x \in [-W,0] \\ 0 & x < -W, \end{cases} \tag{3}
$$

where b is aquifer thickness, Q is the pumping rate from a well located a distance R from the stream bank along the x-axis, Γ [LT^{-1}] is the mass-transfer function across the stream-aquifer interface through the base of the stream, defined as

$$
\Gamma = \beta\left[s(x,y,t) - s_r(t)\right], \;\; x \in [-W,0] \tag{4}
$$

In this equation (4), $s = H_0 - h$ is aquifer drawdown and $s_r = H_0 - h_r$ is stream drawdown, where h is aquifer hydraulic head, 100 h_r is stream stage, and H_0 is initial system hydraulic head, all measured relative to the same datum. Mass exchange across the stream-aquifer interface is characterized by the mass-transfer coefficient, β, defined as the stream conductance $\beta = K'/b'$, where K' is streambed hydraulic conductivity and b' is its thickness. Note that for the NPS case we treat vertical flow across the streambed as a sink/source term in equation (3) defined by the mass-transfer function in equation (4). Also, is the fixed stage models, $s_r \equiv 0$, which is where the model developed in this work departs from fixed-stage models (see below).

105 The flow problem is solved subject to the initial condition

$$
s|_{t=0} = 0, \tag{5}
$$

and the far-field boundary conditions

$$
\lim_{\substack{x \to \pm\infty \\ y \to \pm\infty}} s = 0. \tag{6}
$$

Additionally, continuity conditions for drawdown

110 $$
s_1|_{x=0} = s_2|_{x=0} \tag{7}
$$

$$
s_2|_{x=-W} = s_3|_{x=-W}, \tag{8}
$$

4

and flux

$$\left.\frac{\partial s_1}{\partial x}\right|_{x=0} = \left.\frac{\partial s_2}{\partial x}\right|_{x=0} \tag{9}$$

$$\left.\frac{\partial s_3}{\partial x}\right|_{x=-W} = \left.\frac{\partial s_2}{\partial x}\right|_{x=-W}, \tag{10}$$

115 are enforced at $x = 0$ and $x = -W$.

2.3 Fully-penetrating Stream

A schematic of the conceptual model for the stream-aquifer system with a FPS is shown in Figure 1b. Aquifer drawdown for this case is defined in a piecewise manner as

$$s(x,y,t) = \begin{cases} s_1(x,y,t) & x > 0 \\ s_2(x,y,t) & x < -W \end{cases} \tag{11}$$

120 when flow on the far-side half-space of the aquifer is accounted for. Here, $s_1(x,y,t)$ is the drawdown of the aquifer in the half space with the pumping well, and $s_2(x,y,t)$ is the drawdown in the far side half space. For the case where the flow on the far-side $(x < -W)$ is neglected, only the drawdown on the pumped side is considered.

The boundary condition imposed at the stream-aquifer interface is specified as

$$-K_x \left.\frac{\partial s_1}{\partial x}\right|_{x=0} = \Gamma_1, \tag{12}$$

125 for the pumped half-space, and

$$-K_x \left.\frac{\partial s_2}{\partial x}\right|_{x=-W} = \Gamma_2 \tag{13}$$

on the far side, where the mass-transfer functions Γ_1 and Γ_2 are defined as

$$\Gamma_1 = -\beta \left[s_r(t) - s_1(x,y,t) \right], \; x = 0 \tag{14}$$

$$\Gamma_2 = \beta \left[s_r(t) - s_2(x,y,t) \right], \; x = -W \tag{15}$$

130 for the pumped-side and far-side stream-aquifer interface. Here, we assume that the two interfaces have the same conductance, β. For the case where far-side flow is neglected, $\Gamma_2 \equiv 0$.

2.4 Accounting for Stream Drawdown and Channel Storage

As discussed above, the models of Hantush and Jacob (1955) and Fox et al. (2002) assume that the stream stage is fixed; the stream does not experience drawdown. Here, we develop a model that accounts for stream drawdown. It should be noted that

135 the flow problem defined above is ill-posed for both the NPS and FPS cases because stream drawdown, s_r, is left unspecified in both equations (4) and (14). If the stream is assumed to have fixed stage, as is the case in Hantush and Jacob (1955) and Fox

et al. (2002), $s_r \equiv 0$. From the resulting Robin BC, one can recover both the no-flow and Dirichlet BCs at the stream-aquifer interface by setting $\beta = 0$ and $\beta \to \infty$, respectively.

In this work, we are concerned with the case where the stream stage does not remain fixed but is allowed to respond to

140   pumping (see Figure 1a); the stream is allowed to undergo drawdown in response to aquifer pumping, in which case $s_r \neq 0$. We achieve this by specifying an additional condition at the stream aquifer interface, namely a mass-balance condition applied to the stream, which simply states that the rate of change of mass within the stream equals the rate of mass transfer across the streambed induced by pumping.

For the NPS model, this condition can be mathematically stated by the parsimonious relation.

145
$$C_r \frac{\partial s_r}{\partial t} = \Gamma, \tag{16}$$

whereas for the FPS model

$$C_r \frac{\partial s_r}{\partial t} = \Gamma_1 + \Gamma_2, \tag{17}$$

where C_r is a stream channel storage coefficient, defined such that $C_r \in [0, \infty)$ is a dimensionless measure of the volume of water, δV_w, which flows through a unit area of the streambed, δA_r, per unit change in stream stage, δh_r (i.e.,

150    $C_r = \delta V_w / (\delta A_r \delta h_r)$). It is a measure of the volume contribution of water stored in the stream channel to aquifer flow, and is distinguished here from streambed elastic storage.

For a stream channel with an idealized uniform geometric cross-sectional structure, it is possible to provide simple expressions for this parameter. For example, in the FPS case, the stream channel has a rectangular cross section, with stream width W and aquifer thickness b, $\delta V_w = W \delta y \delta h_r$, $\delta A_r = 2b\delta y$, leading to $C_r = W/b$ if the mass exchange is limited to the stream

155   bank. For the NPS case, where a similar simple geometric profile may be adopted for the cross section of the stream channel, it can be shown that C_r is of the order of unity. For more complex cross-sectional geometries of channels that vary spatially with y, the parameter C_r can be empirically estimated by inversion of the stream and aquifer drawdown data. It is also possible, in principle, to develop empirical functions relating C_r to the dimensionless ratio $\langle W \rangle / h$ of the form $C_r = f(\langle W \rangle / b)$, where $\langle W \rangle$ is some well-defined spatial (in y) average of stream width. Additional research outside the scope of the present work

160   would be needed to develop such empirical relations. It is also easy to imagine the parameter C_r as a (non-linear) function of the stream stage. For our purposes here, in the spirit of parsimony and mathematical tractability, we restrict ourselves to the case where C_r is a constant to develop a first solution that describes stream drawdown in response to aquifer pumping. For our purposes, the effect of flow in the subdomain in the non-pumping half-space is not considered in the following development of the analytical model for FPS and NPS for mathematical tractability.

165   ## 3   Analytical Solutions of the Flow Problem

To solve the flow problem described above, the governing equation is first transformed into a dimensionless form. Details of the nondimensionalization of the governing equations and their solutions may be found in the Appendix. The solutions are given

Hydrology and
Earth System
Sciences
Discussions

Open Access
EGU

below in dimensionless form. The dimensionless variables and parameters that appear in the solution are defined in Table 1. The solutions for s_D and $s_{D,r}$ are obtained using Laplace (in time) and Fourier cosine (in y) transforms.

3.1 Non-Penetrating Stream

The exact solution for aquifer drawdown, in transform space, for the NPS case can be shown (see Appendix for details) to be

$$\bar{\tilde{s}}_D = \frac{2e^{-\eta}}{p\Delta_1} \begin{cases} e^{\eta(1-x_D)}\bar{\tilde{g}}_1(p,\xi,1.0) & \forall x_D > 1 \\ \bar{\tilde{g}}_1(p,\xi,x_D) & \forall x_D \in [0,1] \\ \hat{\eta}\cosh[\hat{\eta}(x_D+W_D)] + \eta\sinh[\hat{\eta}(x_D+W_D)] & x_D \in (-W_D,0) \\ \hat{\eta}e^{\eta(W_D+x_D)} & x_D \leq -W_D, \end{cases} \tag{18}$$

where $\bar{\tilde{s}}_D$ is the Laplace and Fourier cosine transform of s_D, p is the Laplace transform variable, ξ is the Fourier cosine transform variable, $\eta = \sqrt{p+\kappa\xi^2}$, $\hat{\eta} = \sqrt{\eta^2+\zeta}$, $\zeta = p\beta_D/(p+\beta_D^*)$, $\beta_D^* = \beta_D/C_{D,r}$, $\beta_D = \beta/(K_x/R)$ is the dimensionless stream conductance, $W_D = W/R$ is the dimensionless stream channel width, $C_{D,r} = C_r/(RS_s)$ is the dimensionless ration of the stream channel storage coefficient to aquifer elastic storage,

$$\Delta_1 = 2\hat{\eta}\eta\cosh(\hat{\eta}W_D) + (\eta^2+\hat{\eta}^2)\sinh(\hat{\eta}W_D), \tag{19}$$

$$\bar{\tilde{g}}_1(p,\xi,x_D) = \hat{\eta}e^{\eta x_D}\cosh(\hat{\eta}W_D) + \bar{\tilde{g}}_2(p,\xi,x_D)\sinh(\hat{\eta}W_D), \text{ and} \tag{20}$$

$$\bar{\tilde{g}}_2(p,\xi,x_D) = \eta\cosh(\eta x_D) + (\hat{\eta}^2/\eta)\sinh(\eta x_D). \tag{21}$$

The corresponding solution for stream drawdown is given by

$$\bar{\tilde{s}}_{D,r} = \frac{\bar{\tilde{s}}_D(p,\xi,x_D)}{1+p/\beta_D^*}, \quad x_D \in (-W_D,0), \tag{22}$$

where $\bar{\tilde{s}}_{D,r}$ is the Laplace and Fourier cosine transform of dimensionless stream drawdown $s_{D,r}$. Upon inversion from transform space, Equation (22) may be used to compute stream drawdown, in addition to stream depletion, induced by pumping from a well completed in a confined aquifer. Space-time stream and aquifer drawdown are obtained by numerical inversion of the Fourier cosine and Laplace transforms using numerical quadrature and the Stehfest (1970) algorithm as implemented within the Wolfram Mathematica environment.

3.2 Fully-Penetrating Stream

3.2.1 Flow on both sides of stream

As shown in the Appendix D, the exact solution for the FPS model, allowing for flow on both sides of the stream, is given by

$$\bar{\tilde{s}}_D = \frac{2e^{-\eta}}{p\Delta_2} \begin{cases} e^{-\eta(x_D-1)}\bar{\tilde{g}}_3(p,\xi,1.0) & \forall x_D > 1 \\ \bar{\tilde{g}}_3(p,\xi,x_D) & \forall x_D \in [0,1] \\ p\beta_D\beta_D^*e^{\eta(W_D+x_D)} & x_D \leq -W_D, \end{cases} \tag{23}$$

where $\tilde{\bar{s}}_D$ is the Laplace and Fourier cosine transform of aquifer drawdown, s_D,

$$\tilde{\bar{g}}_3(p,\xi,x_D) = \chi_1 \cosh(\eta x_D) + \chi_2 \sinh(\eta x_D), \tag{24}$$

$$\chi_1 = \frac{\Delta_2}{\beta_D + \eta} + p\beta_D^* \beta_D, \tag{25}$$

$$\chi_2 = \frac{\beta_D \Delta_2}{\eta(\beta_D + \eta)} - p\beta_D^* \beta_D, \text{ and} \tag{26}$$

195 $$\Delta_2 = p(\beta_D + \eta)\left[2\beta_D^* \eta + p(\beta_D + \eta)\right]. \tag{27}$$

The corresponding stream drawdown solution in transform space is

$$\tilde{\bar{s}}_{D,r}(p,\xi) = \frac{2e^{-\eta}}{p\Delta_2} \frac{\beta_D^*(\chi_1 + p\beta_D \beta_D^*)}{p + 2\beta_D^*}, \tag{28}$$

in transform space. The space-time solution, a function of t_D and y, is obtained numerically as stated previously.

3.2.2 Flow on pumped side of stream only

200 When there is no flow across the far-side stream-aquifer interface, with $\Gamma_2 \equiv 0$, the solution for the FPS solution can be reduced to

$$\tilde{\bar{s}}_D = \frac{2e^{-\eta}}{p\Delta_3^*} \begin{cases} \tilde{\bar{g}}_5(p,\xi,x_D) & \forall x_D \leq 1 \\ e^{-\eta x_D} \tilde{\bar{g}}_5(p,\xi,1.0) & \forall x_D > 1 \end{cases} \tag{29}$$

where $\tilde{\bar{s}}_D$ is the Laplace and Fourier cosine transform of s_D, $\Delta_3^* = \eta + \zeta$, $\tilde{\bar{g}}_5(p,\xi,x_D) = \cosh(\eta x_D) + (\zeta/\eta)\sinh(\eta x_D)$, and ζ is as defined previously. The corresponding solution for dimensionless stream drawdown is

205 $$\tilde{\bar{s}}_{D,r}(p,\xi) = \left[1 - \chi\left(1 - \frac{1}{\eta p \beta_D}\right)\right]\frac{e^{-\eta}}{p\Delta_3^*}, \tag{30}$$

which upon inversion gives stream drawdown as a function of time, t_D, and position along the stream channel, y_D. As mentioned previously, the inversion is performed numerically in the Wolfram Mathematica environment.

3.3 Stream Depletion Solution

Stream depletion, Q_r [L³T⁻¹], defined as the volume rate of flow captured from the stream by a pumping well, is obtained

210 simply by integrating the point-wise streambed flux along the length of the stream. The point-wise depletion flux, q_r, in dimensionless form, is

$$q_{D,r} = C_{D,r}\frac{\partial s_{D,r}}{\partial t_D} \tag{31}$$

where $q_{D,r} = q_r/(2\pi b R/Q)$. In the Laplace- and Fourier-cosine transform domain, equation (31) becomes $\tilde{\bar{q}}_{D,r} = pC_{D,r}\tilde{\bar{s}}_{D,r}$.

Inverting the Fourier cosine inverse transform yields (Povstenko, 2015)

215 $$\bar{q}_{D,r} = pC_{D,r}\int_0^\infty \tilde{\bar{s}}_{D,r}\cos\xi x_D \, d\xi. \tag{32}$$

Therefore,

$$
\bar{Q}_{D,r} = \frac{C_{D,r}}{\pi} \begin{cases} \displaystyle\int_0^\infty p\bar{s}_{D,r}\,\mathrm{d}y_D & \text{for FPS and} \\[2ex] \dfrac{1}{b_D}\displaystyle\int_0^\infty \int_{-W_D}^0 p\bar{s}_{D,r}\,\mathrm{d}x_D\,\mathrm{d}y_D & \text{for NPS,} \end{cases}
\tag{33}
$$

where $Q_{D,r} = Q_r/Q$. Equation (33) includes improper integrals, which take a long time to evaluate numerically. Additionally, there may be a practical limit on the stream reach that contributes appreciable amounts of water to the well over the pumping

220   period. Hence, a definite integral over the interval $y_D \in [0, L_D]$, may be more practical. Using the late-time drawdown approximation of Cooper Jr and Jacob (1946), namely, $s_D = -\gamma/2 - \ln(u)$ where s_D is dimensionless drawdown, $u = r_D^2/(4\alpha t_D)$, $r_D^2 = (x_D - 1)^2 + y_D^2$, α is the hydraulic diffusivity K/S_s, and $\gamma \simeq 0.577216$ is Euler's constant, one can determine the radius of influence, R_∞, of the pumping well by considering a depression cone centered about the well ($x_D = 1$) and defining R_∞ as $s_D|_{r_D = R_{D,\infty}} = 0$. This leads to

225   $$R_{D,\infty} = A t_D^{1/2},\tag{34}$$

where $A = \sqrt{4\alpha}e^{-\gamma/4} \approx 1.73\sqrt{\alpha}$. Then $L_D \approx R_{D,\infty}$ can be set when evaluating Equation (33). In Figure 2 we compare the $Q_{D,r}$ curves with $L_D = R_{D,\infty}$ given above versus the arbitrary upper bound of $L_D = 10^5$. The two curves are nearly identical with a maximum relative error (RE) of less than 10% at the early time. For $t_D > 1$, the RE is less than 2%. The CPU time shows that the setting $L_D = R_{D,\infty}$ computes faster than the use of $L_D = 10^5$.

230   ## 3.4   Model Verification

To check the correctness of the analytical solutions developed above, a verification exercise was undertaken by comparing these solutions with a numerical solution based on the finite element method (FEM). A 3D FEM model was built for comparison with the NPS case and to evaluate the significance of vertical flow. The stream overlying the aquifer was allowed to drain through the streambed and generate vertical flow. The domain is set as above with $z_D \in [0, 1.5]$. As mentioned above, the conceptual

235   model comprises three isotropic layers, namely the aquifer layer with $z_D \in [0, 1]$, the streambed layer with $z_D \in (1, 1 + b'_D]$ with $x_D \in [-W_D, 0]$ and $y_D \in [0, 10^5]$, and the stream layer with $z_D \in (1 + b'_D, 1.5]$ with $x_D \in [-W_D, 0]$ and $y_D \in [0, 10^5]$. The drawdown computed with the 3D FEM model is vertically averaged. Finer meshes were assigned near the stream and pumping well, ~~while a coarser mesh was used elsewhere~~. The hydraulic parameter values used for the comparison were set to $C_{D,r} = 25$, $\beta_D = 10$, $b'_D = 0.01$, and $W_D = 0.5$. The streambed storage was set the same as the aquifer and $K' = 0.1K_x$.

240   In the case of the FPS with a fully penetrating pumping well, the vertical flow is negligible and a 2D model in the (x_D, y_D) plane is sufficient to describe the flow behavior. The numerical solution was developed in a domain with $x_D \in [-10^5, 10^5]$ and $y_D \in [0, 10^5]$. The flow domain was divided into multiple zones: the pumped aquifer zone: $x_D \in [0, 10^5]$, aquifer zone on the far side: $x_D \in [-2b'_D, -10^5]$, the stream zone: $x_D \in [-b'_D, -b'_D - W_D)$, and streambed zones: $x_D \in [0, -b'_D)$ and $[-b'_D - W_D, -2b'_D - W_D)$, where b'_D is the dimensionless streambed thickness defined as b'/R. Figure 3 shows the aquifer

245   drawdown curves predicted by the (a) NPS and (b) FPS solutions versus the FEM solution. The observation points were
        established at $(x_D, y_D) = (0.1, 0), (0.25, 0), (0.5, 0)$. The results show that the semi-analytical and FEM solutions agree well
        with negligible residuals. Additionally, Butler Jr et al. (2001) tested the assumptions of the NPS model by comparing it with
        the seven-layer MODFLOW model. They found that the NPS assumptions are valid when the relative penetration (ratio of
        stream penetration to aquifer thickness) is less than 85%. For the Cal Poly stream-aquifer system that motivated this study, the
250   relative penetration is 50%.

4   Model Predicted Behavior

4.1   Aquifer and Stream Drawdown Response

Aquifer and stream drawdown predicted by the solutions of NPS and FPS with its special case ($\Gamma_2 = 0$) are shown in Figures
4 (a) and (b), respectively. The models for the case of an impermeable barrier(Ferris et al., 1962), Theis (1935), Hantush
255   (1965), and Fox et al. (2002) are included as limiting cases for comparison. The models of Hantush (1965) and Fox et al.
        (2002) correspond to the limiting case of infinite stream channel storage and no stream drawdown. The limiting solution of an
        impermeable barrier proposed in Ferris et al. (1962) shown in Figure 4(b) is for a semi-infinite flow domain with a no-flow
        fully-penetrating boundary at the stream-aquifer interface.

        The predicted aquifer drawdown response shows three phases that are commonly observed in dual-storage media such as
260   unconfined aquifers (Neuman, 1974; Malama, 2011; Tartakovsky and Neuman, 2007; Mishra and Neuman, 2010; Mishra and
        Kuhlman, 2013; Malama, 2014; Lin et al., 2019) and dual-porosity media (Warren and Root, 1963; Streltsova, 1983; De Smedt,
        2011; Lin and Yeh, 2021). The three phases are termed early-, intermediate-, and late-time. During early-time, aquifer response
        follow the Theis (1935) model and stream drawdown response is virtually imperceptible as water flows primarily from aquifer
        elastic storage. The onset of intermediate-time is marked by significant departure of aquifer drawdown from that predicted by
265   Theis (1935) and aquifer drawdown is lower than it would be in the absence of stream recharge. The stream initially serves
        as a near-infinite store of water and aquifer drawdown closely follows that predicted by the limiting solutions of Fox et al.
        (2002) and Hantush (1965), appearing to approach steady-state before beginning to increase again as the stream stage begins
        to respond significantly to pumping. If pumping were to cease during the early part of intermediate-time, the models of Fox
        et al. (2002) and Hantush (1965) would be sufficient to describe system behavior. The higher stream storage coefficient, $C_{D,r}$,
270   the longer this quasi-static phase persists. As pumping continues, the aquifer drawdown response transitions into late-time
        behavior characterized by increasing aquifer and stream drawdown response; the depression cone has propagated to the edge
        of the stream, capturing water directly from stream channel storage. Depending on the initial stage of the stream, stream
        drawdown would lead to drying up of the stream at late times, and the model developed here would transition into one with
        a no-flow condition at the streambed. For the NPS model, the predicted aquifer drawdown behavior transitions back into an
275   infinite aquifer state of Theis (1935) with the streambed forming a segment of the upper no-flow boundary.

        The dependence of aquifer and stream drawdown on stream channel storage, $C_{D,r}$, as predicted on the pumped aquifer
        side $(0.5, 0)$ and the unpumped aquifer side $(-1.5, 0)$ is depicted in Figures 5 (a), (b), and (c), as well as (d) and (e), respectively.

Hydrology and
Earth System
Sciences

Discussions

Open Access

EGU

The models of Fox et al. (2002) and Hantush (1965), which assume a fixed stream stage and correspond to the case of infinite stream channel storage, are included for comparison for the cases of NPS and FPS with $\Gamma_2 = 0$. Increasing the values of $C_{D,r}$

280   have the effect of prolonging the intermediate phase and increasing the delay in the response of the stream stage to pumping. Streams with high discharge and stage are associated with high values of $C_{D,r}$, and would require prolonged pumping to respond to the drawdown to the transition to the late-time phase. This may take several days, which explains why such streams are typically treated as fixed-stage boundaries. On the unpmped aquifer side (Figures 5d and e), the drawdown of the FPS with $\Gamma_2 = 0$ is not plotted due to the assumption of an infinite reserve of the stream. This shows the results similar to those

285   given in the pumped aquifer, but the case of $C_{D,r} \to \infty$ for the FPS solution is zero because the pumped water comes from the pumped aquifer and the stream. The dependence of aquifer and stream drawdown on the streambed conductance on the pumped aquifer side and the unpumped aquifer side, β_D is depicted in Figure 6. Large values of β_D indicate a strong stream-aquifer hydraulic connection with aquifer drawdown that shows the three phases discussed above. As the value of β_D decreases, aquifer behavior approaches the no-flow solution, with the limiting value of $\beta_D = 0$, corresponding to a no-flow boundary. Stream stage

290   responsiveness increases with increasing values of β_D, leading to decreasing lag times between stream and aquifer responses.

4.2   Stream Depletion Behavior

The predicted SDR is illustrated in Figure 7, where we explore the effect of $C_{D,r}$ on the $Q_{D,r}$ predicted by (a) NPS solution, (b) FPS solution, and (c) FPS solution with $\Gamma_2 = 0$. Generally, for all finite values of $C_{D,r}$, the depletion rate, $Q_{D,r}$, increases initially with time before reaching a peak rate followed by a subsequent decline. This behavior has been previously highlighted

295   in the literature by Zlotnik (2004). For $C_{D,r} \to \infty$, the maximum depletion rate stays fixed indefinitely with all water captured by the pumping well coming from the stream recharge. For finite values of $C_{D,r}$, the depletion rate reaches a peak value of $Q_{D,r} \leq 1.0$, with a unimodal distribution pattern, indicating that the peak depletion rate is only a fraction of the pumping rate even at late-time, with the rest of the water coming from aquifer storage. As $C_{D,r}$ increases, the stream contributes increasing proportions of the water abstracted by the pumping well and the curves of $Q_{D,r}$ are closer to the limiting case of $C_{D,r} \to \infty$.

300   Figure 8 shows the effect of β_D on the behavior of $Q_{D,r}$ predicted by the models. The figure shows that $Q_{D,r}$ increases with increasing β_D because higher values of β_D mean a higher degree of stream-aquifer connectivity. Increasing β_D has the effect of shifting the $Q_{D,r}$ peaks leftward and upward; that is, increasing β_D leads to increased peak depletion, with the peak occurring earlier.

5   Drawdown Derivative Analysis

305   The drawdown derivative analysis is a useful tool to diagnose the change in flow behavior by plotting the curve of $\partial s_D / \partial \ln(t_D)$ for the aquifer flow response or $\partial s_{D,r} / \partial \ln(t_D)$ for the flow response of the stream, because it drastically improved the sensitivity to flow conditions (Bourdet et al., 1983; Chow, 1952; Ferroud et al., 2018, 2019). Figure 9 shows the temporal drawdown derivative curve predicted by the (a) NPS and (b) FPS solutions in the aquifer located at (0.5, 0) and those predicted by (c) the NPS and (d) the FPS solutions in the stream located at (-0.5, 0) by varying the values of $C_{D,r}$ from 10 to 100. As can be

Hydrology and
Earth System
Sciences
Discussions

Open Access

EGU

310 seen in the figure, $C_{D,r} = \infty$ represents the case of fixed stage of river water. It shows a hump that the drawdown derivative value steeply rises and falls down to a near-zero value. It is a typical feature of the recharge boundary effect, especially for the Dirichlet-type condition on the recharge boundary Ferroud et al. (2019). However, for the finite value of $C_{D,r}$, the drawdown derivative displays a double humps with a higher peak for the latter, and then it is stable at a constant value. The valleys of the curves represent the starting point of the river that supports the pumped aquifer. This valley pattern can be observed in a

315 dual porosity system, but in this case it represents the transfer of water from the matrix block to the fracture. In general, the entire pattern shown in Figures 9(a) and (b) can be seen as a characteristic of the effect of stream drawdown on the response of aquifer flow. In the stream, there is an immediate sharp increase in the drawdown derivative that gradually declines until it returns to a constant level. Note that the case of $C_{D,r}$ does not appear in the figure for the stream derivative because $s_{D,r}$ is constant, leading to the zero value of $\partial s_{D,r}/\partial \ln(t_D)$. On the other hand, Figure 10 demonstrates the temporal drawdown

320 derivative curves generated by the (a) NPS and (b) FPS solutions at (0.5, 0) and those predicted by the (c) NPS and (d) FPS solutions at (-0.5, 0) by changing the values of β_D from 0.1 to 1. It shows patterns similar to those of the above figure. As can be seen, when β is zero, the river stage will not charge due to pumping. Moreover, the steady-state pattern for the case of $\beta_D = 0$ represents the radial flow in the aquifer. For the case of NPS, zero β means that the atop the river has no impact on the aquifer and the pumped water is mainly recharged from the storage of the aquifer, while for the case of FPS, it means an impermeable

325 layer near the pumping well. Overall, these curve features can be helpful in identifying the change in stream drawdown once pump-induced drawdown data are obtained near a stream.

6 Application to Field Observations

To test the hypothesis that streams respond to groundwater pumping, we passively monitored the response of a stream-aquifer system to groundwater pumping for irrigation. The null hypothesis in this case is that streams act as constant-head boundaries

330 or as sources of the mass-transfer type with fixed stage, supplying recharge to an aquifer indefinitely during groundwater pumping. In the following, we provide evidence from field observation that a stream in hydraulic contact with a pumped aquifer, experiences transient drawdown in response to the pumping. We also use observations of stream drawdown, in addition to aquifer drawdown data, to estimate aquifer hydraulic properties, stream conductance, and the newly introduced finite stream storage coefficient C_r.

6.1 Study Site Description

The study site is situated in the agricultural fields of the California Polytechnic State University (Cal Poly), San Luis Obispo, located along the California central coast. The site is an alluvial basin underlain with a shallow confined gravel and sand aquifer underlain with metavolcanic bedrock. It is situated at the northern edge of the greater San Luis Obispo aquifer where the water-bearing geologic formations that comprise recent (Quaternary) alluvium, Paso Robles Formation, and Pismo Formation. The

340 metavolcanic bedrock is locally interpreted to belong to the non-water-bearing Franciscan assemblage. The groundwater basin in which the aquifer is situated has been designated as medium priority in the implementation of the Sustainable Groundwater

Management Act (SGMA) passed in the state of California in 2014. Hence, the modeling, data, and results presented here have great implications for an aquifer of significant social relevance.

345   The aquifer is confined and bounded above by a thin near-surface layer of variably saturated clay or clay-rich sediment of very low permeability. This layer constitutes the upper confining unit (upper aquitard) and has a thickness of 11 m. The aquifer is confined from below at a depth of about 24 m by metavolcanic bedrock of unknown thickness. The aquifer has a nominal uniform thickness of $b = 11$ m, as determined from drill logs for well installation. A stream, Stenner Creek, flows across the study site on top of the aquifer in a nearly northwest-to-southeast direction cutting across the entire thickness of the confining layer overlying the aquifer. As will become clear in the following, the stream is in direct hydraulic connection with the aquifer.

350   The streambed is of the same sand and gravel formation as the aquifer, and the stream has minimal penetration of the aquifer. During the summer low flows, the discharge rate of the stream is on the order of $Q_s \sim 5 \times 10^{-4}$ m^3/s.

6.2   Passive Monitoring of Aquifer Pumping

An irrigation well, which serves as the pumping well in this study, has a diameter of 8 inches (~ 0.2 m) and is located about 60 m southwest of the stream, as depicted in Figure 11. It is completed throughout the thickness of the aquifer and is used

355   to pump confined aquifer regularly on a fortnightly schedule at a constant rate of $Q = 138$ gpm (8.58×10^{-3} m^3/s). Aquifer drawdown response to pumping was continuously monitored with transducers in the pumping well and a nearby abandoned well located across the stream about 10 m from the bank as shown on the map. A piezometer 100 m west of the pumping well was also instrumented for monitoring aquifer response. This piezometer and the abandoned well serve as the aquifer drawdown observation wells in this study. It is installed at about the interface between the top of the aquifer and the overlying

360   clay-clayey confining unit. To monitor the stream stage, pressure transducers (Stenner-P1, P2, and P3) were placed in the stream channel in stilling wells without penetrating the streambed at three locations. Two additional stream channel monitoring stations downstream of Stenner-P3 were instrumented with pressure transmitters connected to CR300 data loggers (Campbell Scientific, Inc.) and are marked Stenner-P4 and P5.

    The stream stage was continuously monitored at 15-minute intervals. The time series (hydrographs) of the aquifer water

365   levels in the two observation wells and stream stage at five locations, relative to the long-term background levels, are plotted in Figure 12. The time series of drawdown data have been denoised using the singular spectrum analysis and detrended using the ensemble empirical mode decomposition method to remove the unfavorable noises from the diurnal evapotranspiration signal and the trend due to rainfall events. These functions can be found in the built-in functions in the Python package called pyts.decomposition and PyEMD, respectively. Six pumping events recorded during the spring and summer irrigation seasons

370   of 2022 are highlighted. Due to instrument malfunction, not all episodes of pumping are recorded by each of the monitoring stations. In addition, the six pumping events specifically occurred on March 16 at 9:35, April 27 at 7:12, May 31 at 13:53, June 23 at 9:30, July 18 at 12:05, and August 8 at 7:22 in 2022.

Hydrology and
Earth System
Sciences
Discussions
Open Access
EGU

6.3   Observed Transient Aquifer and Stream Drawdown

Aquifer drawdown recorded in the observation well is shown in Figure 13 for the six tests highlighted previously. The figure

375   shows (a) log-log and (b) semi-log plots of the observed drawdown. The figure also shows in (c) the log-time derivative of the
drawdown data computed numerically using central differences. The recovery data are also included for completeness. The
drawdown data show a general shift in aquifer drawdown behavior of the course of the observation period. The least overall
drawdowns were recorded in the first of the pumping periods of March 16 to March 18, while the largest were recorded in the
last reported pumping period. This behavior is reflective of the decrease in the amount of water stored in the stream channel

380   from the spring high flows to the summer low flows. As stated previously, a small value of the parameter C_r is associated with
larger aquifer drawdowns in the neighborhood of a stream.

In addition to the shift in behavior observed from test to test, for any given test, the transient aquifer response generally
shows the three phases predicted by the model developed in this work, namely early-, intermediate-, and late-time behavior.
These phases are most evident in the latter tests (4,5,6) that are associated with small values of the parameter C_r. The earlier

385   tests (1,2,3), when the stream channel has the most water (large C_r) primarily show the early- and intermediate phases as the
stream acts more like a fixed-stage boundary. Even for the earlier tests, the intermediate phase does not show the constant
late-time drawdown predicted by the models of Hantush and Jacob (1955) and Fox et al. (2002). It is clear from these data that
the parameter changes significantly over the course of the irrigation season, being dependent on stream stage over such long
time scales. However, for the relatively short duration of each test (48 hours), we treat C_r as constant due to the relatively small

390   stream stage responses induced by each test (see below).

The plot of the log-time derivative of aquifer drawdown, $\partial s/\partial \ln(t)$, shown in Figure 13(c) reveals more clearly the three
phases described above, as well as the changes in the stream storage coefficient over the course of the irrigation season and the
six tests. The general temporal behavior of the derivative of aquifer drawdown as depicted in this figure also captures well the
general temporal pattern predicted by the model for different values of the parameter C_r, as shown in Figure 9. The derivative

395   generally increases with time before reaching an initial peak value during the early-time phase of the drawdown response. This
is followed by a general decrease of the slope associated with the contribution of flow from stream recharge, with the slope
attaining a local minimum. This decrease in the derivative observed in the data and predicted by the model is characteristic
of the intermediate-time drawdown response. Figure 10 displays the drawdown derivative curves as changing the value of β_D
with fixing $C_{D,r} = 25$. The same patterns can be observed as shown in Figure (9) due to the effect of $C_{D,r}$. If $C_{D,r}$ is finite and

400   β_D is greater than nil, a similar feature of the drawdown derivative would be observed from the finite storage stream model.

Observed stream stage drawdown data are shown in Figure 14. The response of the aquifer in test 6 is also included in all
the graphs for comparison. The first observation to note is that stream is drawdown is nonzero, coherent, and unambiguous. The
stream clearly does not behave as a fixed-stage boundary or a source term that supplies recharge indefinitely without drawdown.
The second observation is that stream drawdown response occurs significantly later than the aquifer drawdown. All the stream

405   stilling wells are located closer to the pumping well than the aquifer observation well but all start showing drawdown response

at much later times (about an hour later) than the aquifer observation well. This delayed stream response confirms the model predictions presented above.

6.4   Drawdown Analysis and Parameter Estimation

Based on the configuration of the stream and aquifer aquifer at the study site, the NPS solution was used to identify the
410   hydraulic parameters of the aquifer, namely, K_x, κ, and S_s, as well as the streambed conductance, β, and the stream channel storage coefficient, C_r. The solution proposed in this study was coupled with the Levenberg-Marquardt optimization algorithm as implemented in MATLAB through the lsqcurvefit function. The purpose of parameter identification was to minimize the sum of the residuals between the observation drawdown and the predicted drawdown. The objective function Z is defined as

$$Z = \min_{\{K_x, S_s, \kappa, \beta, C_r\}} \sum_{n=1}^{N} [s_{\text{obs}}, (x, y, t_n) - s(x, y, t_n; K_x, S_s, \kappa, \beta, C_r)]^2 \tag{35}$$

415   where N is the total number of temporal drawdown observations, $s_{\text{obs}}(x, y, t_n)$ measured drawdown at location (x, y) at time t_n, and $s(x, y, t_n; K_x, S_s, \kappa, \beta, C_r)$ are the corresponding model computed values given the set of parameters $\{K_x, S_s, \kappa, \beta, C_r\}$. The convergence criterion of equation (35) is set to $Z < 1 \times 10^{-4}$ m. The hydraulic parameters were log-transformed to to constrain the optimization procedure to the positive space of the parameter values.

Additionally, estimated values of hydraulic parameters were checked against published values of geologic materials with
420   similar sediment composition to ensure reliability. The aquifer at the study site is predominantly sand and gravel; therefore, the reasonable range for hydraulic conductivity K_x is $[10^{-6}, 10^{-3}]$ m/s, with $K_y = \kappa K_x$ where $\kappa \sim 1.0$. The possible range for S_s is $[10^{-6}, 10^{-3}]$ m^{-1}, and $\beta > 10^{-9}$ s^{-1}. The value of C_r is bounded only by the log-transformation during the parameter estimation procedure; no published values are available in the hydrogeology literature because the parameter was first introduced in this work. It is expected, however, that this parameter would generally be greater than specific yield in unconfined
425   aquifer settings, and storativity, in confined settings.

In this work, parameter estimation is conducted by considering only drawdown data from the aquifer observation well and the stream stilling well Stenner-P1. The pumping well is located at $R = 62.2$ m and has x-y coordinates $(62.2, 0.0)$ m. The stream observation location Stenner-P1 is located in the middle of the stream channel at $(-0.75, 183.1)$ m, whereas the observation well location is on the far-side of the stream at $(-15.1, 193.6)$ m. The stream channel had an average width of
430   about $w = 1.5$ m during the Spring-Fall period of 2022 when the data analysed here were collected. The aquifer has an average thickness of 11 m, estimated from drilling logs of the pumping and irrigation wells. In all the tests analysed, water was pumped at a constant rate of $Q = 135$ gallons per minute (gpm) to irrigate one half of a lemon orchard for 24 hours, and the other half for another 24-hour period for a total of 48 hours of pumping. However, the pumping rate increases slightly to about 138 gpm at the start of the second 24-hour irrigation period, which has the effect of changing the trajectory of transient drawdown
435   response. Hence, for this work, only data from the first 24 hours (1440 min) of pumping are analysed for the purpose of parameter estimation. Recovery phase data are not considered here in order to simplify the analysis.

Figure 15 shows the best fits of the NPS model to the observation well (aquifer) drawdown data for the six tests highlighted above. The results are plotted on (a) log-log, (b) semi-log, and (c) linear scales. The corresponding estimated parameter values

for the model fits to data that minimize the objective function defined previously are summarized in Table 2. All the model fits to
440 the aquifer drawdown data were obtained with values of $K_x = 8.31 \times 10^{-5}$ m/s for hydraulic conductivity and $S_s = 1.46 \times 10^{-5}$
m^{-1} for specific storage. These values were obtained with test 6 data and then held fixed in the subsequent analyses. Only
parameters κ, β, and C_r were allowed to vary among all the subsequent analyses of tests 1-6.

Figure 15 also includes (in d, e, and f) the predicted stream drawdown behavior at Stenner-P1 using the parameter values
in Table 2 from analysis of aquifer drawdown. These model predictions are compared to the observed stream drawdown. It
445 is clear the the observed stream drawdown shows significant departure from the behavior predicted on the basis of hydraulic
parameters estimated with aquifer drawdown only. This is particularly the case for test 4 data depicted in Figure 15(d). Hence,
stream drawdown data where analysed separately and the resulting model fits to observed transient behavior are shown in Figure
16 on (a) log-log, (b) semi-log, and (c) linear scales. Model fits show a marked improvement and the resulting parameter values
are summarized in Table 3. These values are appreciably different from those estimated from aquifer drawdown only, which
450 may be attributed to system heterogeneity (more on this in the discussion below). The estimated values of the anisotropy ratio,
κ, are in the range of 0.591 to 1.09, which implies that the aquifer is only modestly anisotropic. The parameter β was also
estimated with only modest variation among the tests.

In the analysis of aquifer drawdown data, the most significant parameter change among the 6 tests was observed in the
stream storage coefficient C_r. The results are plotted in Figure 17, showing the temporal behavior over the course of the six
455 pumping tests. For each individual test, C_r was taken to be constant, but there was clear and consistent decrease from test 1
to 6. This decrease of C_r over the course of the pumping season correlates with a reduction in the river stage and discharge
during the dry season. This variation notwithstanding, the results, indicate that the stream storage is finite and estimable and
may be treated as fixed only for a relatively short duration corresponding to a single pumping period of 24-hours.

7 Discussion

460 This work sought to resolve the stream depletion paradox where streams in hydraulic contact with an aquifer undergoing
pumping from a well experience depletion without stage decline or drawdown. Models were developed by introducing a mass
balance condition at the stream-aquifer interface and a finite stream storage coefficient, which allow the stream to show a
transient drawdown response to groundwater pumping. These are the first analytical models in the hydrogeology literature to
accomplish this overcoming the limitation of published analytical models that assume streams to be fixed-head boundaries or
465 source terms. For simplicity and mathematical tractability, stream velocity was neglected in the theory presented here. The
resulting mathematical solutions show that predicted aquifer drawdown has a three-phase response characteristic of a two-
storage flow system, namely, (1) an early-time response associated with water released from aquifer elastic storage, (2) an
intermediate-time response where water is released from a combination of stream and aquifer storage, and (3) a late-time phase
where water is withdrawn primarily from stream storage, with stream stage showing decline or drawdown. The intermediate-
470 and late-time phases are characterized by aquifer drawdown departure from the steady-state drawdown behavior predicted by
models with a fixed stream stage.

Hydrology and
Earth System
Sciences
Open Access
EGU

Discussions

Direct observations of stream drawdown at multiple locations at the study site clearly demonstrate that streams cannot in general be treated as strictly constant head boundary conditions or as mass transfer source terms with fixed stage. This also implies that streams should more generally be treated as having finite storage where they cannot supply water to pumping wells

475 indefinitely. The mathematical solution developed in this work, with the application of a mass conservation condition in the stream channel and the introduction of a finite stream storage coefficient, C_r, was used to estimate aquifer and stream hydraulic parameters by fitting the model to observed aquifer and stream drawdown. In particular, the NPS solution was used because it best matches the stream configuration relative to the aquifer to the extent that Stenner Creek at the study site only minimally penetrates the aquifer.

480 The transient behavior of aquifer drawdown data shows the features predicted by the mathematical model, with early-time, intermediate, and late-time phases clearly evident in tests 5 and 6; these two tests correspond to the *low* stream storage coefficient, when stream discharge and stage where approaching the summer low flows. The earlier tests, conducted when the stream discharge and stage were relatively high, and the observed aquifer drawdown response shows only the early-time and intermediate-time phases; the 24-hour test period was not sufficiently long for the aquifer to transition into late-time behavior,

485 though there were hints of this behavior in data from test 4. Analysis of time derivatives of the data supports this observation and shows close correspondence between the general pattern of the model predicted derivative behavior with the observed behavior for different values of the stream storage coefficient.

Qualitatively, stream drawdown behavior also conforms to model predicted temporal behavior, being significantly delayed in response compared to aquifer response, even though the aquifer observation well is farther from the pumping well. The

490 highest stream drawdown was recorded in Stenner-P1 which was also the farthest from the pumping well. This suggests that the aquifer may be anisotropic. Quantitatively, the model was found to fit the observed aquifer drawdown very well with R^2-values larger that 90%. Parameter estimation directly from aquifer drawdown, by minimizing the sum of squared residuals between these data and model predictions, yielded reasonable values of hydraulic conductivity, K_x, specific storage, S_s, and hydraulic anisotropy, $\kappa = K_y/K_x$, for an aquifer made up of unconsolidated sand and gravel. In analyzing aquifer drawdown

495 for parameter estimation, the same K_x and S_s values were found to lead to very good fits ($R^2 > 90\%$) of the model to drawdown. Because the observed drawdown suggested anisotropic conditions, an attempt was made to estimate this parameter for each of the tests, yielding only modest variations in κ. Estimated stream conductance values, β, also showed only modest variation (coefficient of variation of $\sim 8\%$) among the tests.

The stream channel storage coefficient, C_r, shows the greatest and most consistent variation among the six tests, being

500 largest for test 1, which was conducted in March 2022, and lowest for test 6 conducted in August of the same year. Test 1 coincided with high stream discharge (flow rate) and stage following the end of the rainy season, whereas test 6 was conducted in the middle of the summer dry season, when stream flow was predominantly dictated by baseflow recession. During the earlier tests, the stream acts as a large water storage source of recharge, hence the large values of C_r and the induced stream drawdown relative to (as a fraction of) stream stage is much lower than later in the dry season; aquifer drawdown may be approximated

505 by the solutions of Hantush (1965) and Fox et al. (2002) as it may be perceived to approach steady state. However, the fact that the stream was not acting as a fixed stage boundary or source is clear from the induced stream drawdown, and in the

change in the observed aquifer drawdown, particularly during the intermediate and late-time stages of tests 4-6. Additionally, the parameter identification for these field tests showed that the stream channel storage in Stenner Creek decreases as the dry season progresses, which also coincides with the irrigation season where the frequency of pumping events tends to increase.
510 This can have significant implications for the sustainable management of water resources in interacting stream-aquifer systems with heavy groundwater abstraction.

The predicted transient stream drawdown behavior, using parameter values in Table 2 that were estimated from aquifer drawdown data, was found to be significantly mismatched with observed stream drawdown. This was particularly the case for test 4, with tests 5 and 6 showing improved alignment between model predictions and observed behavior albeit with poor model
515 fit to data. This necessitated separate analysis of stream drawdown data leading to greatly improved model fits to data (see Figure 16) but with parameter values that are appreciably different from those estimated using aquifer drawdown observations. This suggests that the aquifer and streambed may be heterogeneous and that estimation of their equivalent homogeneous hydraulic properties would require joint inversion of aquifer and stream drawdown data. For the purposed of the present work, it is sufficient to demonstrate that aquifer and stream hydraulic properties are estimable from both stream and aquifer drawdown
520 data, while highlighting the need for further analysis.

8 Conclusions

The data and modeling results of this work demonstrate that aquifer flow models with a fixed stream stage boundary condition or source term underestimate aquifer drawdown and overestimate the capacity of a stream to buffer aquifer drawdown through continuous recharge. Streams are demonstrated to have finite and estimable channel storage and undergo both depletion and
525 drawdown when an aquifer in close proximity is pumped. This is especially critical in aquifer systems subjected to prolonged groundwater abstraction, which can lead to the drying of streambeds, as has been observed in many groundwater basins with irrigated agriculture. Models with fixed stream stage overestimate the available groundwater supply from the stream because of their inherent assumption of infinite stream storage. The results of this work have implications for sustainable groundwater management. The model developed may be used to not only predict the stream depletion rate but also the decline of stream
530 stage referred to as stream drawdown. Additional work is needed to incorporate stream discharge (or velocity) in the model and to conduct longer pumping tests than reported herein in order to better constrain parameter estimates.

Appendix A: Non-dimesionalization of NPS Flow Problem

On the basis of Table 1, the governing equation, in dimensionless form, for the case of NPS, is as follows.

$$\frac{\partial s_D}{\partial t_D} = \frac{\partial^2 s_D}{\partial x_D^2} + \kappa \frac{\partial^2 s_D}{\partial y_D^2} + f_D, \tag{A1}$$

535 where $s_{D,i} = s_{D,i}(x_D, y_D, t_D)$ is dimensionless aquifer drawdown, s_i/H_c, in the ith sub-domain, with $i = 1, 2, 3$, $H_c = Q/(2\pi b K_x)$ is a system characteristic head, $x_D = x/R$ and $y_D = y/R$ are dimensionless distances in the x and y directions,

$t_D = t/T_c$ is dimensionless time, $T_c = R^2/\alpha_x$ is a characteristic system time, $\alpha_x = K_x/S_s$ is aquifer horizontal hydraulic diffusivity in the x-direction, $\kappa = K_y/K_x$ is the anisotropy ratio in the horizontal plane, and $f_D = f_D(x_D, y_D, t_D)$ is the piecewise dimensionless sink/source term defined by

540

$$f_D = \begin{cases} -2\delta(x_D - 1)\delta(y_D) & x_D > 0, \\ \Gamma_D & x_D \in (-W_D, 0), \\ 0 & x_D \leq -W_D. \end{cases} \tag{A2}$$

Here $\Gamma_D = \Gamma/[Q/(2\pi R^2)] = \beta_D(s_{D,2} - s_{D,r})$ is the dimensionless mass-transfer function at the stream-aquifer interface. A more complete list of dimensionless variables and relevant parameters is provided in Table 1. Equation (A1) is solved subject to the initial condition

$$s_D|_{t_D=0} = 0, \tag{A3}$$

545 and the far-field boundary conditions

$$\lim_{\substack{x_D \to \pm\infty \\ y_D \to \pm\infty}} s_D = 0. \tag{A4}$$

The dimensionless continuity conditions at $x_D = 0$ and $x_D = -W_D$ are specified as

$$s_{D,1}|_{x_D=0} = s_{D,2}|_{x_D=0}, \tag{A5}$$

$$s_{D,2}|_{x_D=-W_D} = s_{D,3}|_{x_D=-W_D}, \tag{A6}$$

550 for drawdown, and

$$\left.\frac{\partial s_{D,1}}{\partial x_D}\right|_{x_D=0} = \left.\frac{\partial s_{D,2}}{\partial x_D}\right|_{x_D=0} \tag{A7}$$

$$\left.\frac{\partial s_{D,2}}{\partial x}\right|_{x_D=-W_D} = \left.\frac{\partial s_{D,3}}{\partial x}\right|_{x_D=-W_D} \tag{A8}$$

for flux. In dimensionless form the stream-mass-balance condition becomes

$$C_{D,r}\frac{\partial s_{D,r}}{\partial t_D} = \beta_D(s_{D,2} - s_{D,r}), \tag{A9}$$

555 where $C_{D,r} = b_D C_r/S$ is the dimensionless stream storage coefficient, $s_{D,r} = s_r/H_c$, $\beta_D = \beta R/K_x$ is the dimensionless mass transfer coefficient across the streambed, $S = bS_s$ is aquifer storativity, and $b_D = b/R$ is dimensionless aquifer thickness. Note that C_r/S is simple the ratio of the stream storage coefficient to aquifer storativity. The dimensionless initial condition associated with this mass balance condition is

$$s_{D,r}(t_D = 0) = 0. \tag{A10}$$

560 **Appendix B:** **Derivation of the NPS Solution**

Applying the Laplace and Fourier cosine transforms to to equations A1 and A2 leads to

$$\eta^2 \tilde{\bar{s}}_D = \frac{\partial^2 \tilde{\bar{s}}_D}{\partial x_D^2} + \begin{cases} -\dfrac{2}{p}\delta(x_D - 1) & x_D > 0 \\ \pm\chi\tilde{\bar{s}}_{D,2} & x_D \in (-W_D, 0) \\ 0 & x_D \leq -W \end{cases}, \tag{B1}$$

where $\eta = \sqrt{p + \kappa\xi^2}$, $\chi = \beta_D p/(p + \beta_D^*)$, p is the Laplace transform parameter, and ξ is the Fourier cosine transform parameter. The problem domain in (x_D, y_D) dimensionless plane is symmetrical with x_D-axis; therefore, the problem domain

565 $y_D \in (-\infty, \infty)$ can simply be reduced to $y_D \in [0, \infty)$. Therefore, the symmetric boundary conditions for s_D can be described by no-flow Neumann-type boundary conditions, i.e., $\partial s_D/\partial y_D$ at $y_D = 0$. The transformed governing equations for the NPS solution are

$$\eta^2 \tilde{\bar{s}}_{D,1} = \frac{d^2 \tilde{\bar{s}}_{D,1}}{dx_D^2} - \frac{2}{p}\delta(x_D - 1), \qquad\qquad x_D \in [0, \infty), y_D \in [0, \infty) \tag{B2}$$

$$\hat{\eta}^2 \tilde{\bar{s}}_{D,2} = \frac{d^2 \tilde{\bar{s}}_{D,2}}{dx_D^2}, \qquad\qquad x_D \in [-W_D, 0), y_D \in [0, \infty) \tag{B3}$$

570 $$\eta^2 \tilde{\bar{s}}_{D,3} = \frac{d^2 \tilde{\bar{s}}_{D,3}}{dx_D^2}, \qquad\qquad x_D \in (-\infty, -W_D), y_D \in [0, \infty) \tag{B4}$$

where $\hat{\eta}^2 = \eta^2 + \chi$.

The transformed dimensionless stream-mass-balance condition from equation (A9) is

$$p\tilde{\bar{s}}_{D,r} = \beta_D^*(\tilde{\bar{s}}_{D,2} - \tilde{\bar{s}}_{D,r}), \tag{B5}$$

which can be rearranged as

575 $$\tilde{\bar{s}}_{D,r} = \left(\frac{\beta_D^*}{p + \beta_D^*}\right)\tilde{\bar{s}}_{D,2}. \tag{B6}$$

The far-field conditions are

$$\lim_{x_D \to \pm\infty} \tilde{\bar{s}}_{D,1} = 0. \tag{B7}$$

The transformed continuity conditions from equations (A5) – (A7), respectively, are

$$\tilde{\bar{s}}_{D,1}\big|_{x_D=0} = \tilde{\bar{s}}_{D,2}\big|_{x_D=0}, \tag{B8}$$

580 $$\tilde{\bar{s}}_{D,2}\big|_{x_D=-W_D} = \tilde{\bar{s}}_{D,3}\big|_{x_D=-W_D}, \tag{B9}$$

$$\frac{d\tilde{\bar{s}}_{D,1}}{dx_D}\bigg|_{x_D=0} = \frac{d\tilde{\bar{s}}_{D,2}}{dx_D}\bigg|_{x_D=0}, \tag{B10}$$

$$\frac{d\tilde{\bar{s}}_{D,2}}{dx}\bigg|_{x_D=-W_D} = \frac{d\tilde{\bar{s}}_{D,3}}{dx}\bigg|_{x_D=-W_D}. \tag{B11}$$

Given the jump discontinuity introduced by the Dirac Delta source at $x_D = 1$, the solution for $\tilde{\bar{s}}_{D,1}$ is piecewise, having the form

$$585 \quad \tilde{\bar{s}}_{D,1} = \begin{cases} A_1 e^{\eta x_D} + A_2 e^{-\eta x_D} & \forall x_D \in (1, \infty) \\ A_3 \cosh(\eta x_D) + A_4 \sinh(\eta x_D) & \forall x_D \in [0, 1) \end{cases} \tag{B12}$$

where $A_1 - A_4$ are undetermined coefficients. From the farfield homogeneous boundary condition, it follows that $A_1 = 0$. The general solutions of equations (B3) and (B4) can be readily obtained and respectively give

$$\tilde{\bar{s}}_{D,2} = A_5 \cosh(\hat{\eta} x_D) + A_6 \sinh(\hat{\eta} x_D) \tag{B13}$$

$$\tilde{\bar{s}}_{D,3} = A_7 e^{\eta x_D} + A_8 e^{-\eta x_D} \tag{B14}$$

590   where A_5 to A_8 are coefficients to be determined by applying the boundary conditions defined above. From the farfield boundary conditions stated in equation (B7), the coefficients $A_1 = A_8 \equiv 0$.

In addition to the boundary conditions already specified above, jump conditions across the Dirac Delta source at $x_D = 1$ are required to determine these coefficients. The jump conditions are

$$\tilde{\bar{s}}_{D,1}\big|_{x_D = 1^+} = \tilde{\bar{s}}_{D,1}\big|_{x_D = 1^-}, \tag{B15}$$

$$595 \quad \frac{\mathrm{d}\tilde{\bar{s}}_{D,1}}{\mathrm{d}x_D}\bigg|_{x_D = 1^+} = \frac{\mathrm{d}\tilde{\bar{s}}_{D,1}}{\mathrm{d}x_D}\bigg|_{x_D = 1^-} - \frac{2}{p}, \tag{B16}$$

where $x_D = 1^{\pm} = \lim_{\delta \to 0} 1 \pm \delta$, where δ is a small interval across the Dirac Delta source. These two conditions enforce head or drawdown continuity at $x_D = 1$ and define the flux discontinuity, respectively. Applying these two conditions to the solution in Equation (B12) leads to

$$A_2 e^{-\eta} = A_3 \cosh(\eta) + A_4 \sinh(\eta), \text{ and} \tag{B17}$$

$$600 \quad -A_2 e^{-\eta} = A_3 \sinh(\eta) + A_4 \cosh(\eta) - \frac{2}{p\eta}. \tag{B18}$$

Also, applying continuity conditions at $x_D = 0$ gives

$$A_3 = A_5, \text{ and} \tag{B19}$$

$$\eta A_4 = \phi A_6 = \hat{\eta} A_6. \tag{B20}$$

Finally, applying continuity conditions at $x_D = -W_D$ leads to

$$605 \quad A_5 \cosh(\hat{\eta} W_D) - A_6 \sinh(\hat{\eta} W_D) = A_7 e^{-\eta W_D}, \text{ and} \tag{B21}$$

$$-A_5 \sinh(\hat{\eta} W_D) + A_6 \cosh(\hat{\eta} W_D) = \frac{\eta}{\hat{\eta}} A_7 e^{-\eta W_D)}. \tag{B22}$$

Hydrology and
Earth System
Sciences
Discussions

Open Access

EGU

Equations (B17)-(B22) fully define the linear system of equations needed to determine the coefficients A_2–A_7. These equations were solved in the Wolfram Mathematica environment and checked manually, yielding the coefficients as

$$A_2 = \frac{2}{p\eta}\left(\cosh(\eta) - \frac{\hat{\eta}}{\Delta_1}e^{-\eta}\hat{\chi}_2\right), \tag{B23}$$

$$A_3 = A_5 = \frac{2}{p\Delta_1}e^{-\eta}\hat{\chi}_1, \tag{B24}$$

$$A_4 = \frac{2\hat{\eta}}{p\eta\Delta_1}e^{-\eta}\hat{\chi}_2, \tag{B25}$$

$$A_6 = \frac{2}{p\Delta_1}e^{-\eta}\hat{\chi}_2, \text{ and} \tag{B26}$$

$$A_7 = \frac{2\hat{\eta}}{p\Delta_1}e^{-\eta(1-W_D)} \tag{B27}$$

where

$$\Delta_1 = 2\hat{\eta}\eta\cosh(\hat{\eta}W_D) + \left(\eta^2 + \hat{\eta}^2\right)\sinh(\hat{\eta}W_D), \tag{B28}$$

$$\hat{\chi}_1 = \hat{\eta}\cosh(\hat{\eta}W_D) + \eta\sinh(\hat{\eta}W_D), \text{ and} \tag{B29}$$

$$\hat{\chi}_2 = \eta\cosh(\hat{\eta}W_D) + \hat{\eta}\sinh(\hat{\eta}W_D). \tag{B30}$$

Substituting these coefficients into equations (B12) – (B14), the aquifer and stream drawdown solutions for NPS are obtained and shown in Equations (18) and (22), respectively.

Appendix C: Non-dimensionalization of FPS Flow Problem

The dimensionless governing equations for the FPS bounded by two aquifers are

$$\frac{\partial s_D}{\partial t_D} = \frac{\partial^2 s_D}{\partial x_D^2} + \kappa\frac{\partial^2 s_D}{\partial y_D^2} + f_D, \tag{C1}$$

with

$$f_D = \begin{cases} -2\delta(x_D - 1)\delta(y_D) & x_D > 0, \\ 0 & x_D < -W_D. \end{cases} \tag{C2}$$

Equation (C1) is solved subject to the dimensionless initial condition.

$$s_D|_{t_D=0} = 0, \tag{C3}$$

and far-field boundary condition

$$\lim_{\substack{x_D \to \pm\infty \\ y_D \to \pm\infty}} s_D = 0. \tag{C4}$$

The dimensionless flux boundary conditions at the stream-aquifer interfaces 1 and 2, respectively, are

$$\left.\frac{\partial s_{D,1}}{\partial x_D}\right|_{x_D=0} = \beta_D\left(\left.s_{D,1}\right|_{x_D=0} - s_{D,r}\right), \tag{C5}$$

$$\left.\frac{\partial s_{D,2}}{\partial x_D}\right|_{x_D=-W_D} = \beta_D\left(s_{D,r} - \left.s_{D,2}\right|_{x_D=-W_D}\right) \tag{C6}$$

The dimensionless stream-mass-balance condition becomes

$$C_{D,r}\frac{\partial s_{D,r}}{\partial t_D} = \beta_D\left(\left.s_{D,1}\right|_{x_D=0} - s_{D,r}\right) + \beta_D\left(s_{D,r} - \left.s_{D,2}\right|_{x_D=-W_D}\right). \tag{C7}$$

Equations (C1) – (C7) fully describe the well-posed nondimensional flow problem for a fully penetrating stream considered herein.

Appendix D: Derivation of the FPS Solution

The Fourier cosine transform method can then be used to eliminate y_D; meanwhile, the Laplace transform method can eliminate t_D in Equation (C1). The transformed flow equation for the pumped aquifer ($j=1$) is

$$\eta^2\tilde{\bar{s}}_{D,1} + 2\delta_D(x_D - 1) = \frac{\mathrm{d}^2\tilde{\bar{s}}_{D,1}}{\mathrm{d}x_D^2}, \tag{D1}$$

for $x_D \in [0,\infty), y_D \in [0,\infty)$, and for the aquifer on the other side ($j=2$) is

$$\eta^2\tilde{\bar{s}}_{D,2} = \frac{\mathrm{d}^2\tilde{\bar{s}}_{D,2}}{\mathrm{d}x_D^2}, \tag{D2}$$

for $x_D \in [-W_D, -\infty), y_D \in [0,\infty)$, where $\eta = \sqrt{p + \kappa\xi^2}$ with the Laplace parameter p and Fourier parameter ξ; the over-bar and tilde represent the function the Laplace and Fourier domains, respectively.

Similarly, the dimensionless Laplace-Fourier-domain boundary conditions in x_D-direction are obtained as

$$\lim_{x_D\to\infty}\tilde{\bar{s}}_{D,1} = \lim_{x_D\to-\infty}\tilde{\bar{s}}_{D,2} \equiv 0. \tag{D3}$$

The dimensionless inner boundary conditions at $x_D = 0$ and $-W_D$, respectively, give the following.

$$\left.\frac{\mathrm{d}\tilde{\bar{s}}_{D,1}}{\mathrm{d}x_D}\right|_{x_D=0} = \beta_D(\tilde{\bar{s}}_{D,1} - \tilde{\bar{s}}_{D,r})|_{x_D=0}, \tag{D4}$$

$$\left.\frac{\mathrm{d}\tilde{\bar{s}}_{D,2}}{\mathrm{d}x_D}\right|_{x_D=-W_D} = \beta_D(\tilde{\bar{s}}_{D,r} - \tilde{\bar{s}}_{D,2})|_{x_D=-W_D}. \tag{D5}$$

The dimensionless stream mass-balance condition, equation (C7), in the Laplace-Fourier domain is

$$p\tilde{\bar{s}}_{D,r} = \beta_D^*(\tilde{\bar{s}}_{D,1}|_{x_D=0} - \tilde{\bar{s}}_{D,r}) - \beta_D^*(\tilde{\bar{s}}_{D,r} - \tilde{\bar{s}}_{D,2}|_{x_D=-W_D}). \tag{D6}$$

Rearranging equation (D6), one obtains

$$\tilde{\bar{s}}_{D,r} = \frac{\beta_D^*}{p + 2\beta_D^*}(\tilde{\bar{s}}_{D,1}|_{x_D=0} + \tilde{\bar{s}}_{D,2}|_{x_D=-W_D}). \tag{D7}$$

The jump conditions at $x_D = 1$ are same as equations (D8) and (E7),

$$\tilde{\bar{s}}_{D,1}\big|_{x_D=1^+} = \tilde{\bar{s}}_{D,1}\big|_{x_D=1^-}, \tag{D8}$$

655

$$\frac{\mathrm{d}\tilde{\bar{s}}_{D,1}}{\mathrm{d}x_D}\bigg|_{x_D=1^+} = \frac{\mathrm{d}\tilde{\bar{s}}_{D,1}}{\mathrm{d}x_D}\bigg|_{x_D=1^-} - \frac{2}{p}. \tag{D9}$$

After applying the far-field boundary conditions, the solutions are

$$\tilde{\bar{s}}_{D,1} = \begin{cases} B_2 e^{-\eta x_D} & \forall x \geq 1, \\ B_3 \cosh(\eta x_D) + B_4 \sinh(\eta x_D) & \forall x \in [0,1] \end{cases} \tag{D10}$$

$$\tilde{\bar{s}}_{D,2} = B_5 e^{\eta x_D} \ \forall x_D < -W_D \tag{D11}$$

$$\tilde{\bar{s}}_{D,r} = \frac{\beta_D^*}{p + 2\beta_D^*}(\tilde{\bar{s}}_{D,1}\big|_{x_D=0} + \tilde{\bar{s}}_{D,2}\big|_{x_D=-W_D}) \ \forall x_D \in [-W_D, 0]. \tag{D12}$$

660 where $B_2 - B_5$ are undetermined coefficients. Upon applying the boundary and jump conditions, it can be shown that

$$B_2 = \frac{2}{p\Delta_2}\{\chi_1 \cosh(\eta) + \chi_2 \sinh(\eta)\} \tag{D13}$$

$$B_3 = \frac{2}{p\Delta_2}e^{-\eta}\chi_1 \tag{D14}$$

$$B_4 = \frac{2}{p\Delta_2}e^{-\eta}\chi_2 \tag{D15}$$

$$B_5 = \frac{2}{\Delta_2}\beta_D\beta_D^* e^{\eta(W_D-1)} \tag{D16}$$

665 where $\Delta_2 = p(\beta_D + \eta)[2\beta_D^*\eta + p(\beta_D + \eta)]$. Substituting these coefficients into Equation (D10) leads to the solutions given in equations (23) and (28), for aquifer and stream drawdown.

Appendix E: Derivation of the FPS Solution for $\Gamma_2 = 0$

When $\Gamma_2 = 0$, the FPS solution will ignore the effect of unpumped aquifer. The same integral transformations applied previously are used. For the case for $\Gamma_2 = 0$, we only have to focus on solving the pumped aquifer, giving the following.

670 $$\eta^2 \tilde{\bar{s}}_D + 2\delta_D(x_D - 1) = \frac{\mathrm{d}^2 \tilde{\bar{s}}_D}{\mathrm{d}x_D^2}, \tag{E1}$$

for $x_D \in [0, \infty), y_D \in [0, \infty)$. We drop the subscript for drawdown because there is only one aquifer, that is, the pumped aquifer. The dimensionless Laplace-Fourier-domain boundary conditions in x_D-direction, are obtained as

$$\lim_{x_D \to \infty} \tilde{\bar{s}}_D \equiv 0. \tag{E2}$$

675 $$\frac{\mathrm{d}\tilde{\bar{s}}_D}{\mathrm{d}x_D}\bigg|_{x_D=0} = \beta_D(\tilde{\bar{s}}_D - \tilde{\bar{s}}_{D,r})\big|_{x_D=0}. \tag{E3}$$

The dimensionless stream mass-balance condition is transformed as

$$p\tilde{\bar{s}}_{D,r} = \beta_D^*(\tilde{\bar{s}}_D|_{x_D=0} - \tilde{\bar{s}}_{D,r}). \tag{E4}$$

Solving equation (E4), one can obtain

$$\tilde{\bar{s}}_{D,r} = \frac{\beta_D^*}{p+\beta_D^*}\,\tilde{\bar{s}}_D|_{x_D=0}. \tag{E5}$$

To deal with the Dirac Delta function in equation (E1), the jump conditions in $x_D = 1$ are imposed, that is,

$$\tilde{\bar{s}}_D|_{x_D=1^+} = \tilde{\bar{s}}_D|_{x_D=1^-}, \tag{E6}$$

$$\frac{\mathrm{d}\tilde{\bar{s}}_D}{\mathrm{d}x_D}\bigg|_{x_D=1^+} = \frac{\mathrm{d}\tilde{\bar{s}}_D}{\mathrm{d}x_D}\bigg|_{x_D=1^-} - \frac{2}{p}, \tag{E7}$$

Therefore, The general solutions for $\tilde{\bar{s}}_{D,L}$ and $\tilde{\bar{s}}_{D,R}$ are

$$\tilde{\bar{s}}_D = \begin{cases} C_1 e^{\eta x_D} + C_2 e^{-\eta x_D} & x_D > 1, \text{ and} \\ C_3 e^{\eta x_D} + C_4 e^{-\eta x_D} & x_D \in [0,1), \end{cases} \tag{E8}$$

where $C_1 - C_4$ are undetermined coefficients. From the farfield boundary condition, it follows that $C_1 \equiv 0$. Imposing equations (E3) and (E4) on equation (E8), it can be shown that

$$C_2 = \frac{2}{p\eta\Delta_3}[(p+\beta_D^*)\eta\cosh(\eta) + p\beta_D\sinh(\eta)], \tag{E9}$$

$$C_3 = \frac{2e^{-\eta}(p+\beta_D^*)}{p\Delta_3}, \tag{E10}$$

$$C_4 = \frac{2\beta e^{-\eta}}{\eta\Delta_3}, \tag{E11}$$

where $\Delta_3 = \eta(p+\beta_D^*)+p\beta_D$. From the coefficients obtained above, the dimensionless aquifer and stream drawdown solutions for FPS are given in equations (29) and (30), respectively.

References

Asadi-Aghbolaghi, M. and Seyyedian, H.: An analytical solution for groundwater flow to a vertical well in a triangle-shaped aquifer, Journal of Hydrology, 393, 341–348, https://doi.org/https://doi.org/10.1016/j.jhydrol.2010.08.034, 2010.

700   Bochever, F.: Evaluation of well-field yield in alluvial aquifers: The impact of a partially penetrating stream, Proceedings of VODGEO (Hydrogeology), 13, 84–115, 1966.

Bourdet, D., Whittle, T., Douglas, A., and Pirard, Y.: A new set of type curves simplifies well test analysis, World oil, 196, 95–106, 1983.

Bowen, J., Kroeger, K., Tomasky, G., Pabich, W., Cole, M., Carmichael, R., and Valiela, I.: A review of land–sea coupling by groundwater discharge of nitrogen to New England estuaries: Mechanisms and effects, Applied geochemistry, 22, 175–191,
705   https://doi.org/https://doi.org/10.1016/j.apgeochem.2006.09.002, 2007.

Butler Jr, J. J., Zlotnik, V. A., and Tsou, M.-S.: Drawdown and stream depletion produced by pumping in the vicinity of a partially penetrating stream, Groundwater, 39, 651–659, https://doi.org/https://doi.org/10.1111/j.1745-6584.2001.tb02354.x, 2001.

Butler Jr, J. J., Zhan, X., and Zlotnik, V. A.: Pumping-induced drawdown and stream depletion in a leaky aquifer system, Groundwater, 45, 178–186, https://doi.org/https://doi.org/10.1111/j.1745-6584.2006.00272.x, 2007.

710   Chan, Y.: Improved image-well technique for aquifer analysis, Journal of Hydrology, 29, 149–164, https://doi.org/https://doi.org/10.1016/0022-1694(76)90011-1, 1976.

Chow, V. T.: On the determination of transmissibility and storage coefficients from pumping test data, Eos, Transactions American Geophysical Union, 33, 397–404, https://doi.org/https://doi.org/10.1029/TR033i003p00397, 1952.

Cooper Jr, H. and Jacob, C. E.: A generalized graphical method for evaluating formation constants and summarizing well-field history, Eos,
715   Transactions American Geophysical Union, 27, 526–534, https://doi.org/https://doi.org/10.1029/TR027i004p00526, 1946.

De Smedt, F.: Analytical solution for constant-rate pumping test in fissured porous media with double-porosity behaviour, Transport in Porous Media, 88, 479–489, https://doi.org/https://doi.org/10.1007/s11242-011-9750-9, 2011.

Ferris, J. G., Knowles, D. B., Brown, R., and Stallman, R. W.: Theory of aquifer tests, US Government Printing Office Denver, CO, USA, 1962.

720   Ferroud, A., Chesnaux, R., and Rafini, S.: Insights on pumping well interpretation from flow dimension analysis: The learnings of a multi-context field database, Journal of hydrology, 556, 449–474, https://doi.org/https://doi.org/10.1016/j.jhydrol.2017.10.008, 2018.

Ferroud, A., Rafini, S., and Chesnaux, R.: Using flow dimension sequences to interpret non-uniform aquifers with constant-rate pumping-tests: A review, Journal of Hydrology X, 2, 100 003, https://doi.org/https://doi.org/10.1016/j.hydroa.2018.100003, 2019.

Foglia, L., McNally, A., and Harter, T.: Coupling a spatiotemporally distributed soil water budget with stream-depletion func-
725   tions to inform stakeholder-driven management of groundwater-dependent ecosystems, Water Resources Research, 49, 7292–7310, https://doi.org/https://doi.org/10.1002/wrcr.20555, 2013.

Fox, G. A., DuChateau, P., and Dumford, D. S.: Analytical model for aquifer response incorporating distributed stream leakage, Groundwater, 40, 378–384, https://doi.org/https://doi.org/10.1111/j.1745-6584.2002.tb02516.x, 2002.

Glover, R. E. and Balmer, G. G.: River depletion resulting from pumping a well near a river, Eos, Transactions American Geophysical Union,
730   35, 468–470, https://doi.org/https://doi.org/10.1029/TR035i003p00468, 1954.

Grigoryev, V.: The effect of streambed siltation on well-field yield in alluvial aquifers, Water Supply and Sanitation, 6, 10–l, 1957.

Hantush, M. S.: Wells near streams with semipervious beds, Journal of Geophysical Research, 70, 2829–2838, https://doi.org/https://doi.org/10.1029/JZ070i012p02829, 1965.

Hantush, M. S. and Jacob, C. E.: Non-steady radial flow in an infinite leaky aquifer, Eos, Transactions American Geophysical Union, 36,
735   95–100, https://doi.org/https://doi.org/10.1029/TR036i001p00095, 1955.

Harbaugh, A. W.: MODFLOW-2005, the US Geological Survey modular ground-water model: the ground-water flow process, US Depart-
        ment of the Interior, US Geological Survey Reston, VA, 2005.

Huang, C.-S., Yang, T., and Yeh, H.-D.: Review of analytical models to stream depletion induced by pumping: Guide to model selection,
        Journal of Hydrology, 561, 277–285, https://doi.org/https://doi.org/10.1016/j.jhydrol.2018.04.015, 2018.

740   Huang, C.-S., Wang, Z., Lin, Y.-C., Yeh, H.-D., and Yang, T.: New analytical models for flow induced by pumping in a stream-aquifer system:
        A new Robin boundary condition reflecting joint effect of streambed width and storage, Water Resources Research, 56, e2019WR026 352,
        https://doi.org/https://doi.org/10.1029/2019WR026352, 2020.

Hunt, B.: Unsteady stream depletion from ground water pumping, Groundwater, 37, 98–102, https://doi.org/https://doi.org/10.1111/j.1745-
        6584.1999.tb00962.x, 1999.

745   Hunt, B.: Field-data analysis for stream depletion, Journal of Hydrologic Engineering, 8, 222–225,
        https://doi.org/https://doi.org/10.1061/(ASCE)1084-0699(2003)8:4(222), 2003.

Hunt, B.: Stream depletion in a two-layer leaky aquifer system, Journal of Hydrologic Engineering, 14, 895–903,
        https://doi.org/https://doi.org/10.1061/(ASCE)HE.1943-5584.0000063, 2009.

Intaraprasong, T. and Zhan, H.: A general framework of stream–aquifer interaction caused by variable stream stages, Journal of Hydrology,
750   373, 112–121, https://doi.org/https://doi.org/10.1016/j.jhydrol.2009.04.016, 2009.

Jenkins, C. T.: Techniques for Computing Rate and Volume of Stream Depletion by Wells, Groundwater, 6, 37–46,
        https://doi.org/https://doi.org/10.1111/j.1745-6584.1968.tb01641.x, 1968.

Kollet, S. J. and Zlotnik, V. A.: Stream depletion predictions using pumping test data from a heterogeneous stream–aquifer system (a case
        study from the Great Plains, USA), Journal of Hydrology, 281, 96–114, 2003.

755   Kwon, H.-I., Koh, D.-C., Jung, Y.-Y., Kim, D.-H., and Ha, K.: Evaluating the impacts of intense seasonal groundwater pumping on
        stream–aquifer interactions in agricultural riparian zones using a multi-parameter approach, Journal of Hydrology, 584, 124 683,
        https://doi.org/https://doi.org/10.1016/j.jhydrol.2020.124683, 2020.

Li, Q., Gleeson, T., Zipper, S. C., and Kerr, B.: Too many streams and not enough time or money? Analytical depletion functions for
        streamflow depletion estimates, Groundwater, 60, 145–155, https://doi.org/https://doi.org/10.1111/gwat.13124, 2022.

760   Lin, Y.-C. and Yeh, H.-D.: A lagging model for describing drawdown induced by a constant-rate pumping in a leaky confined aquifer, Water
        Resources Research, 53, 8500–8511, https://doi.org/https://doi.org/10.1002/2017WR021115, 2017.

Lin, Y.-C. and Yeh, H.-D.: An Analytical Model With a Generalized Nonlinear Water Transfer Term for the Flow in Dual-
        Porosity Media Induced by Constant-Rate Pumping in a Leaky Fractured Aquifer, Water Resources Research, 57, e2020WR029 186,
        https://doi.org/https://doi.org/10.1029/2020WR029186, 2021.

765   Lin, Y.-C., Huang, C.-S., and Yeh, H.-D.: Analysis of unconfined flow induced by constant rate pumping based on the lagging theory, Water
        Resources Research, 55, 3925–3940, https://doi.org/https://doi.org/10.1029/2018WR023893, 2019.

Malama, B.: Alternative linearization of water table kinematic condition for unconfined aquifer pumping test modeling and its implications
        for specific yield estimates, Journal of Hydrology, 399, 141–147, https://doi.org/https://doi.org/10.1016/j.jhydrol.2010.11.007, 2011.

Malama, B.: Theory of transient streaming potentials in coupled unconfined aquifer-unsaturated zone flow to a well, Water Resources
770   Research, 50, 2921–2945, https://doi.org/https://doi.org/10.1002/2013WR014909, 2014.

Mishra, P. K. and Kuhlman, K. L.: Unconfined aquifer flow theory: from Dupuit to present, in: Advances in Hydrogeology, pp. 185–202, Springer, 2013.

Mishra, P. K. and Neuman, S. P.: Improved forward and inverse analyses of saturated-unsaturated flow toward a well in a compressible unconfined aquifer, Water Resources Research, 46, https://doi.org/https://doi.org/10.1029/2009WR008899, 2010.

775 Neuman, S. P.: Effect of partial penetration on flow in unconfined aquifers considering delayed gravity response, Water Resources Research, 10, 303–312, https://doi.org/https://doi.org/10.1029/WR010i002p00303, 1974.

Povstenko, Y.: Linear fractional diffusion-wave equation for scientists and engineers, Springer, 2015.

Prudic, D. E., Konikow, L. F., and Banta, E. R.: A new streamflow-routing (SFR1) package to simulate stream-aquifer interaction with MODFLOW-2000, 2004.

780 Refsgaard, J. C., Storm, B., and Clausen, T.: Système Hydrologique Europeén (SHE): review and perspectives after 30 years development in distributed physically-based hydrological modelling, Hydrology Research, 41, 355, https://doi.org/https://doi.org/10.2166/nh.2010.009, 2010.

Stehfest, H.: Algorithm 368: Numerical inversion of Laplace transforms [D5], Communications of the ACM, 13, 47–49, https://doi.org/https://doi.org/10.1145/361953.361969, 1970.

785 Streltsova, T. D.: Well pressure behavior of a naturally fractured reservoir, Society of Petroleum Engineers Journal, 23, 769–780, https://doi.org/https://doi.org/10.2118/10782-PA, 1983.

Tartakovsky, G. D. and Neuman, S. P.: Three-dimensional saturated-unsaturated flow with axial symmetry to a partially penetrating well in a compressible unconfined aquifer, Water Resources Research, 43, https://doi.org/https://doi.org/10.1029/2006WR005153, 2007.

Theis, C. V.: The relation between the lowering of the piezometric surface and the rate and duration of discharge of a well using ground-water
790 storage, Eos, Transactions American Geophysical Union, 16, 519–524, https://doi.org/https://doi.org/10.1029/TR016i002p00519, 1935.

Theis, C. V.: The effect of a well on the flow of a nearby stream, Eos, Transactions American Geophysical Union, 22, 734–738, https://doi.org/https://doi.org/10.1029/TR022i003p00734, 1941.

Tolley, D., Foglia, L., and Harter, T.: Sensitivity Analysis and Calibration of an Integrated Hydrologic Model in an Ir-rigated Agricultural Basin With a Groundwater-Dependent Ecosystem, Water Resources Research, 55, 7876–7901,
795 https://doi.org/https://doi.org/10.1029/2018WR024209, 2019.

Warren, J. and Root, P. J.: The behavior of naturally fractured reservoirs, Society of Petroleum Engineers Journal, 3, 245–255, https://doi.org/https://doi.org/10.2118/426-PA, 1963.

Winter, T. C., Harvey, J. W., Franke, O. L., and Alley, W. M.: Ground water and surface water: a single resource, vol. 1139, US Geological Survey, 1998.

800 Xiong, M., Tong, C., and Huang, C.-S.: A New Approach to Three-Dimensional Flow in a Pumped Confined Aquifer Connected to a Shallow Stream: Near-Stream and Far-From-Stream Groundwater Extractions, Water Resources Research, 57, e2020WR028 780, https://doi.org/https://doi.org/10.1029/2020WR028780, 2021.

Yu, H.-L. and Chu, H.-J.: Understanding space–time patterns of groundwater system by empirical orthogonal functions: a case study in the Choshui River alluvial fan, Taiwan, Journal of Hydrology, 381, 239–247, https://doi.org/https://doi.org/10.1016/j.jhydrol.2009.11.046,
805 2010.

Zipper, S. C., Dallemagne, T., Gleeson, T., Boerman, T. C., and Hartmann, A.: Groundwater pumping impacts on real stream networks: Testing the performance of simple management tools, Water Resources Research, 54, 5471–5486, https://doi.org/https://doi.org/10.1029/2018WR022707, 2018.

Zlotnik, V. A.: A concept of maximum stream depletion rate for leaky aquifers in alluvial valleys, Water Resources Research, 40, https://doi.org/https://doi.org/10.1029/2003WR002932, 2004.

810   Zlotnik, V. A. and Tartakovsky, D. M.: Stream depletion by groundwater pumping in leaky aquifers, Journal of Hydrologic Engineering, 13, 43–50, https://doi.org/https://doi.org/10.1061/(ASCE)1084-0699(2008)13:2(43), 2008.

Zlotnik, V. A., Huang, H., and Butler Jr, J. J.: Evaluation of stream depletion considering finite stream width, shallow penetration, and properties of streambed sediments, 2nd International Conference on Water Resources & Environment Research, 1999.

Hydrology and
Earth System
Sciences
Discussions

Open Access

EGU
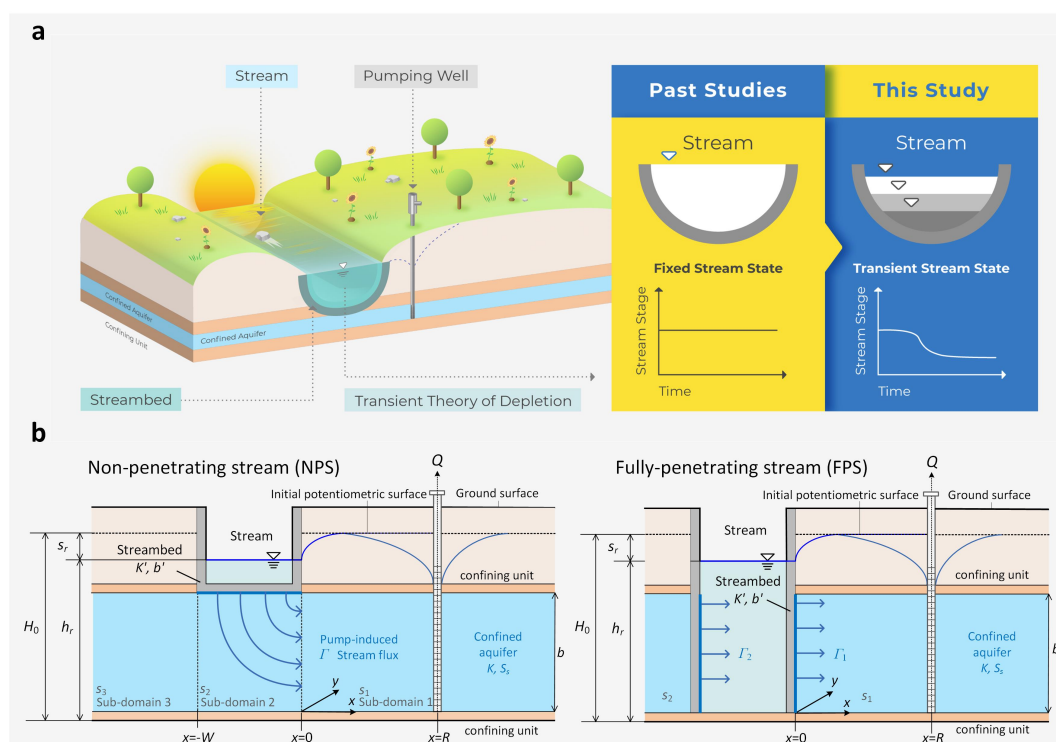
Figure 1. (a) Figure illustrating that the stream stage responds to pumping and (b) the schematic diagram of the conceptual model of the stream-aquifer system used for the NPS and FPS models derived herein.
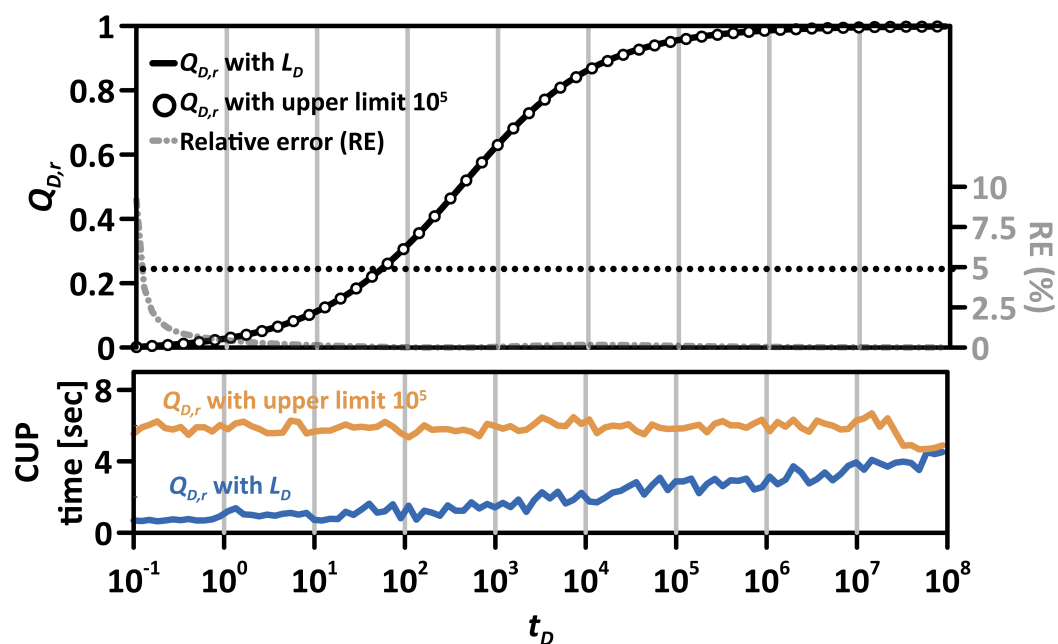
Figure 2. The $Q_{D,r}$ curves showing evaluated depletion integral using upper limit of L_D (solid line) and 10^5 (circle symbol). The relative error curve (dashed line) and associated curves of used CPU time are also included below.
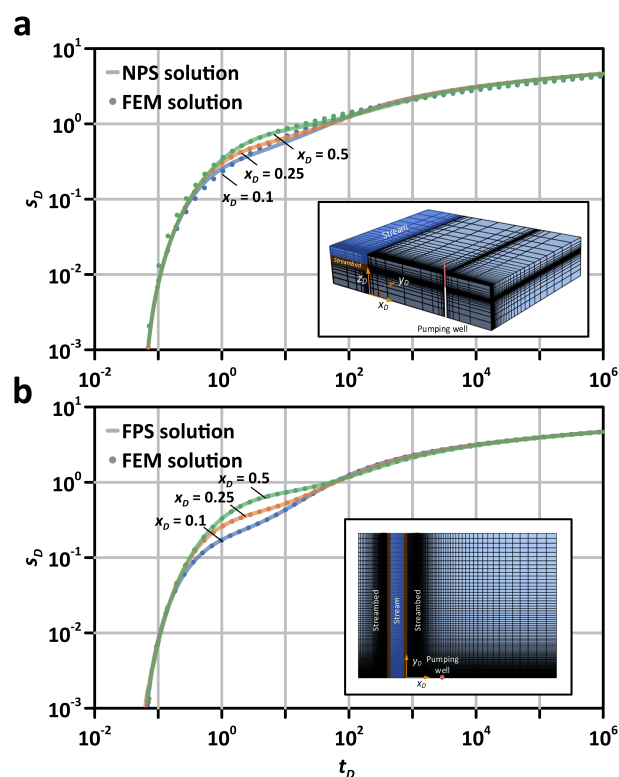
Figure 3. Comparison of the aquifer drawdown curves predicted by the (a) NPS and (b) FPS solutions and FEM solutions based on 3D and 2D model. The visual representations of the meshes near the well used in the 3D and 2D FEM models are included in the bottom right corner of the figure.
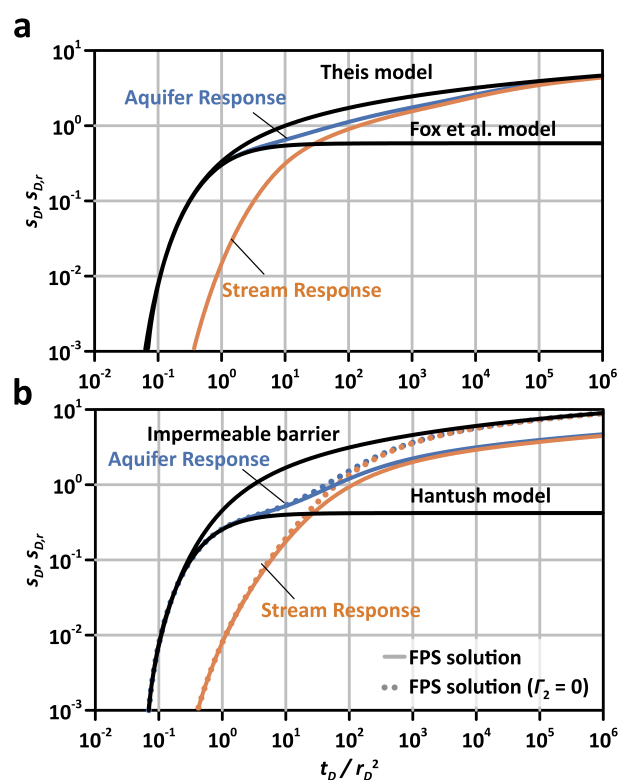
Figure 4. Transient aquifer and stream drawdown response predicted by the (a) NPS and (b) FPS solutions illustrating the stream depletion paradox.
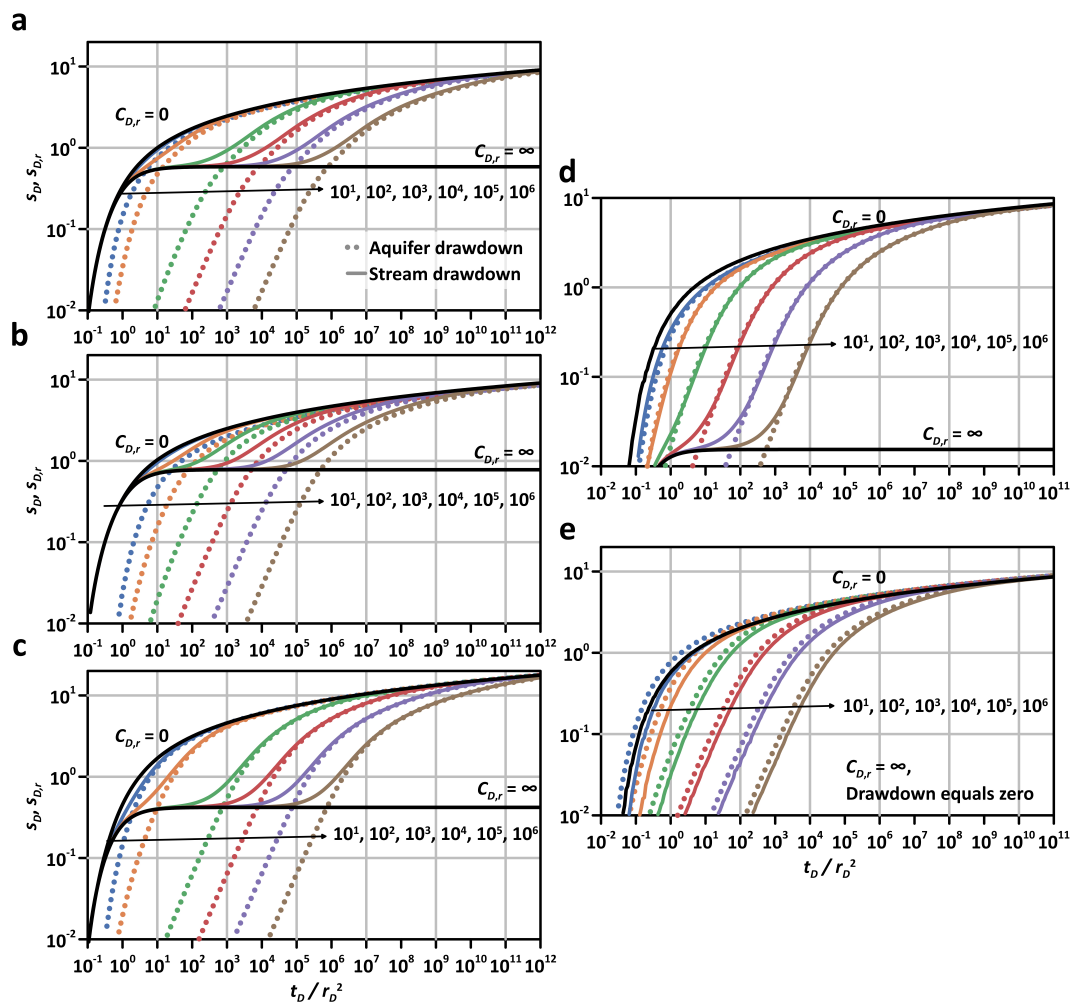
Figure 5. Temporal aquifer and stream drawdowns with different $C_{D,r}$ values predicted by (a) the NPS solution, (b) FPS solution, and (c) FPS solution with $\Gamma_2 = 0$ at (0.5, 0) (i.e., pumped aquifer) and (d) the curves predicted by NPS and (e) FPS solutions at (-1.5, 0) (i.e., unpumped aquifer).
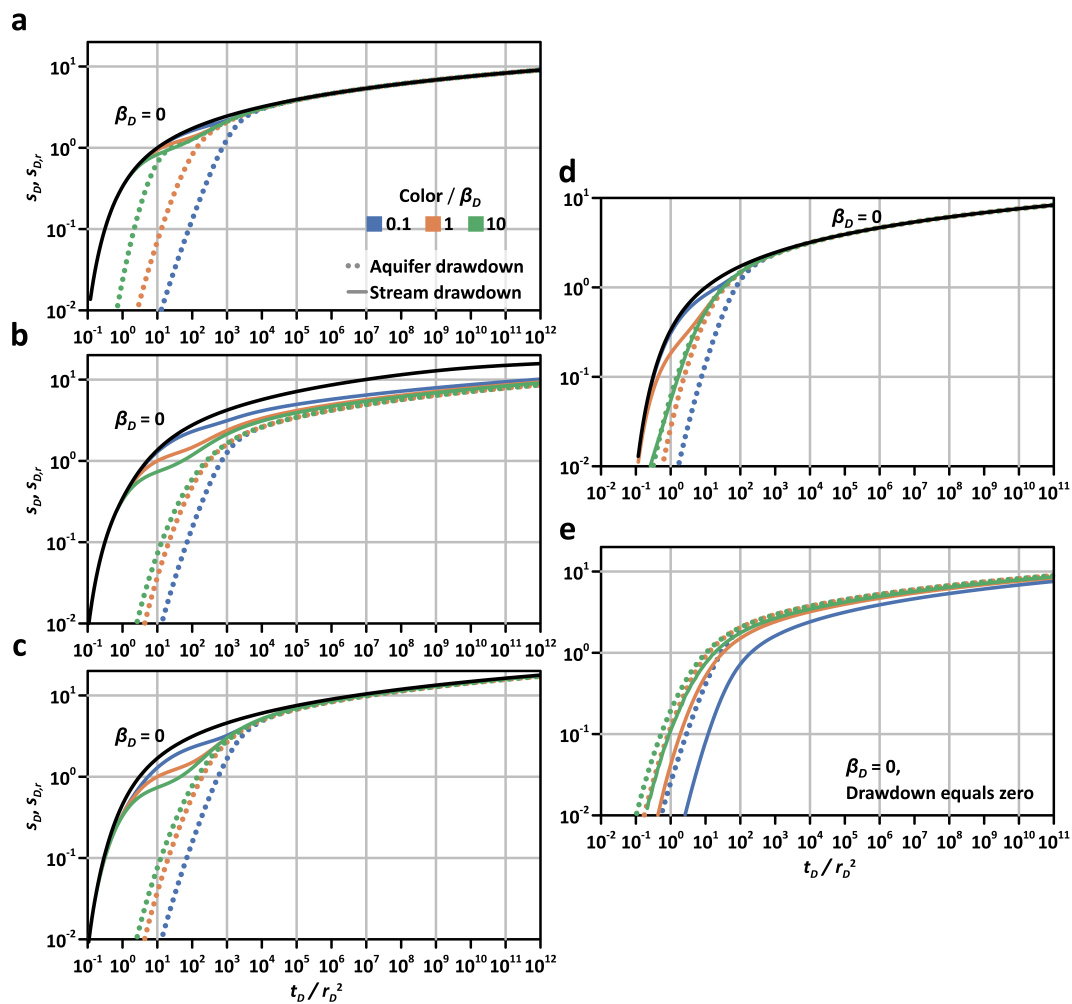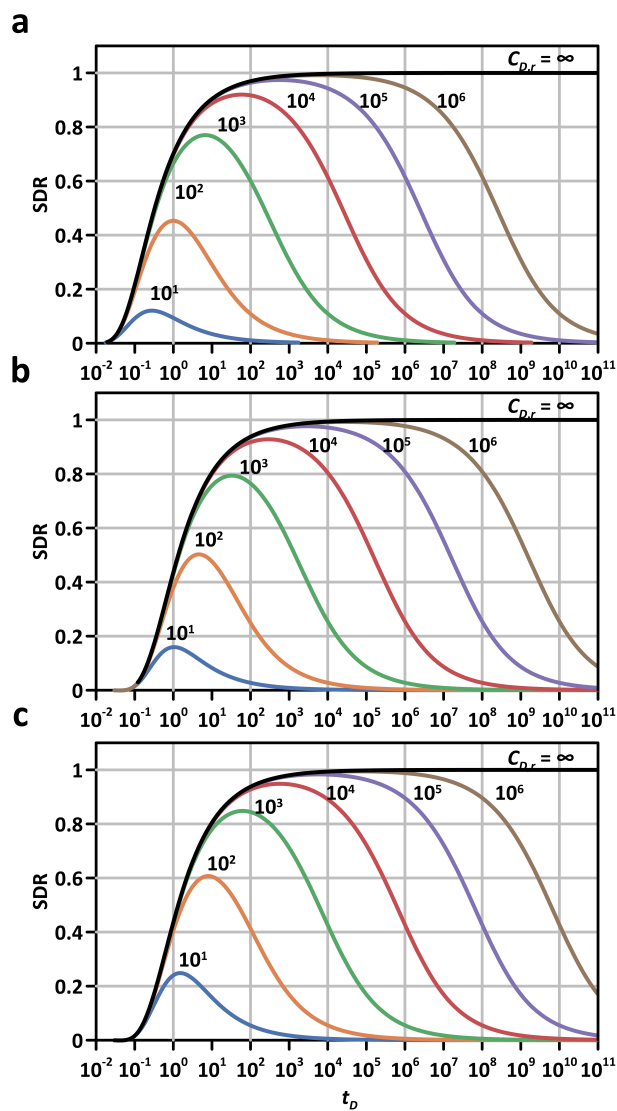
Figure 6. Temporal aquifer and stream drawdowns with different β_D values predicted by (a) the NPS solution, (b) FPS solution, and (c) FPS solution with $\Gamma_2 = 0$ at (0.5, 0) (i.e., pumped aquifer) and (d) the curves predicted by NPS and (e) FPS solutions at (-1.5, 0) (i.e., unpumped aquifer).

Figure 7. Temporal SDR with different $C_{D,r}$ values predicted by (a) the NPS solution, (b) FPS solution, and (c) FPS solution with $\Gamma_2 = 0$.
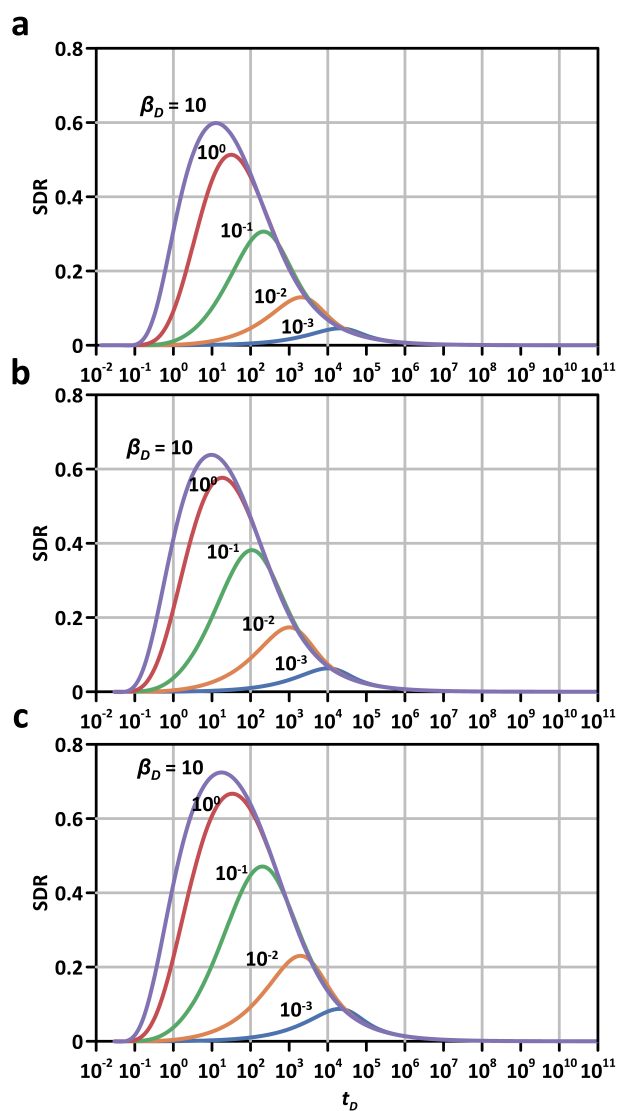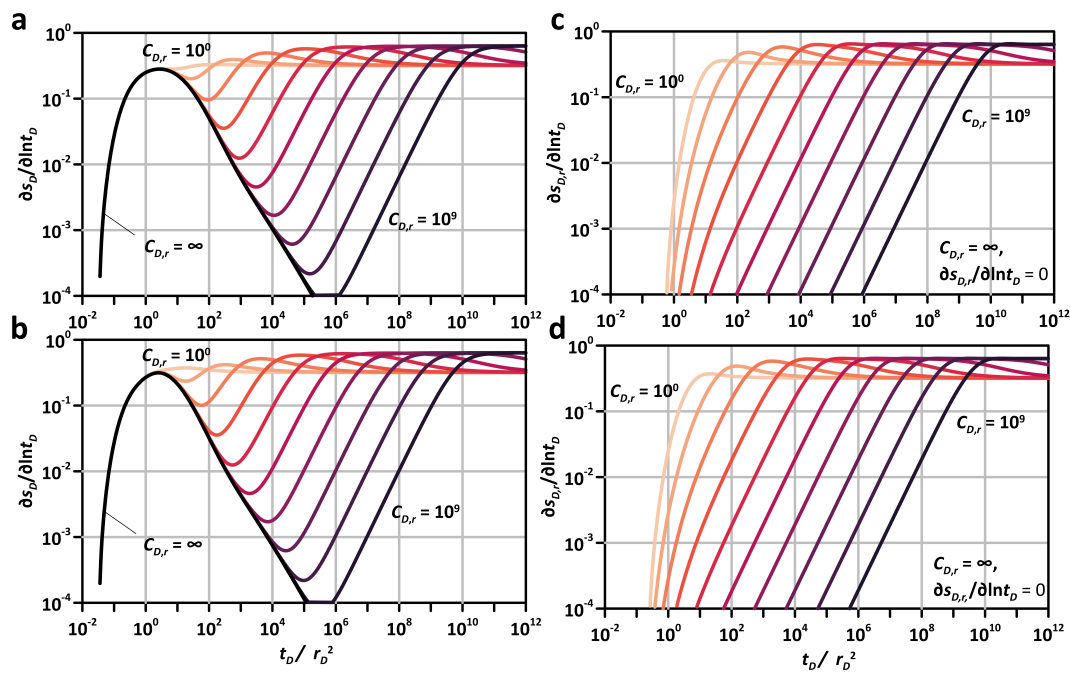
Hydrology and
Earth System
Sciences
Discussions
Open Access
EGU

Figure 8. Temporal SDR with different β_D values predicted by (a) the NPS solution, (b) FPS solution, and (c) FPS solution with $\Gamma_2 = 0$.

Figure 9. Temporal aquifer drawdown derivatives for the cases of (a) NPS and (b) FPS solutions and stream derivatives for the cases of (c) NPS and (d) FPS solutions with varying $C_{D,r}$ values.
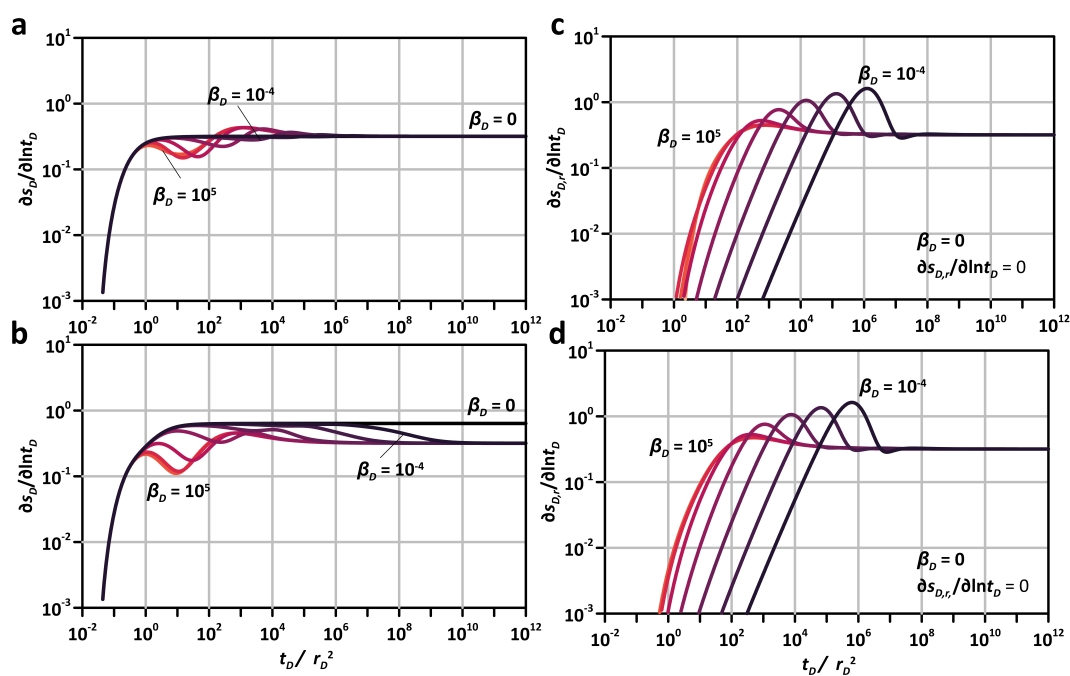
Figure 10. Temporal aquifer drawdown derivatives for the cases of (a) NPS and (b) FPS solutions and stream derivatives for the cases of (c) NPS and (d) FPS solutions with varying β_D values.
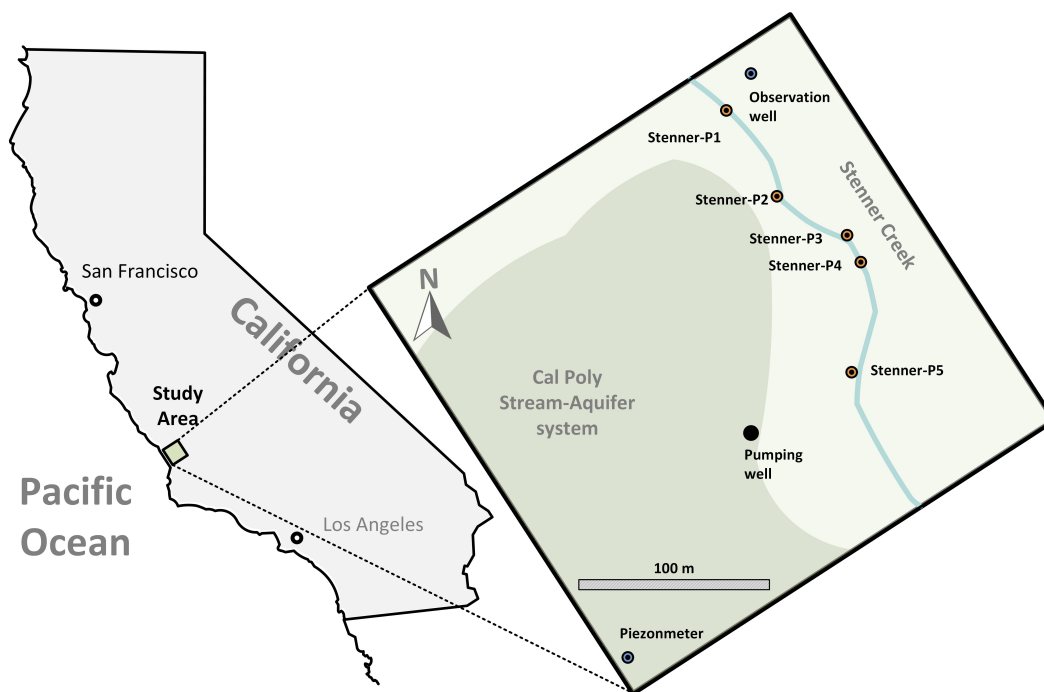
Figure 11. The map of the study site at California Polytechnic State University, San Luis Obispo, showing the observation locations along the stream and the observation well and the aquifer piezometer.
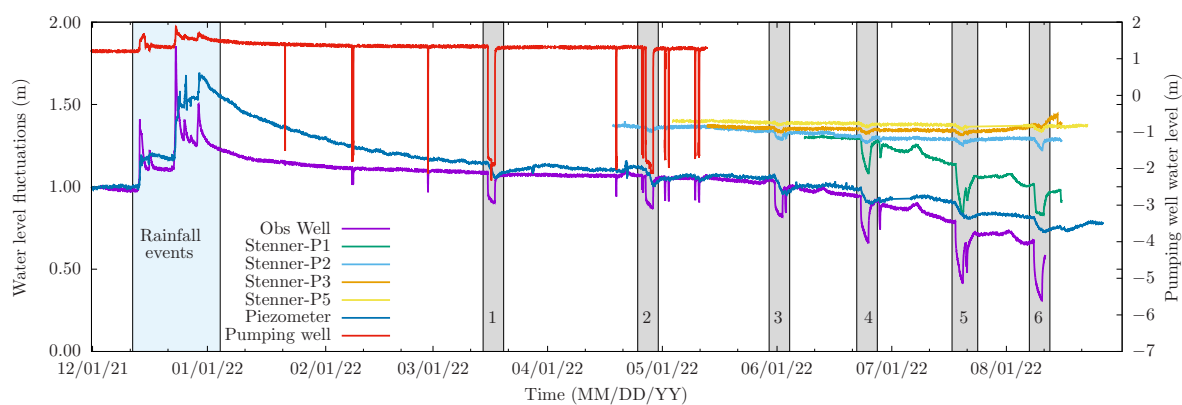
Figure 12. Time series of groundwater and stream stage fluctuations observed in the stream-aquifer system in this work. The six pumping events are colored gray and labeled 1-6.
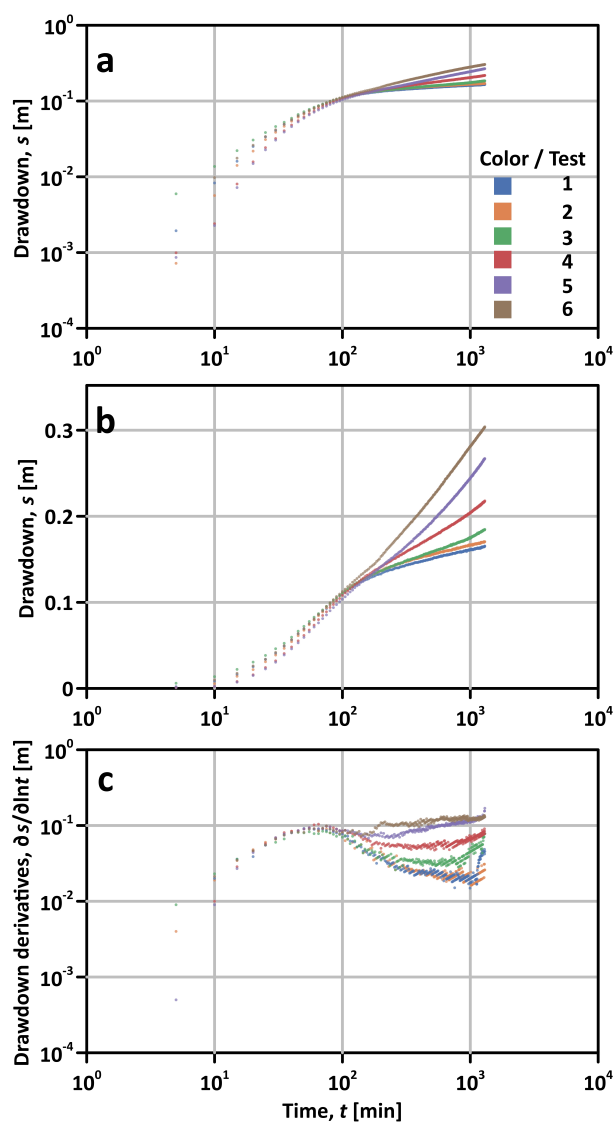
Figure 13. Plots of aquifer drawdown recorded in the observation well on the (a) log-log and (b) semi-log scale. The logarithmic time derivative of drawdown is plotted in (c) using centered differencing.
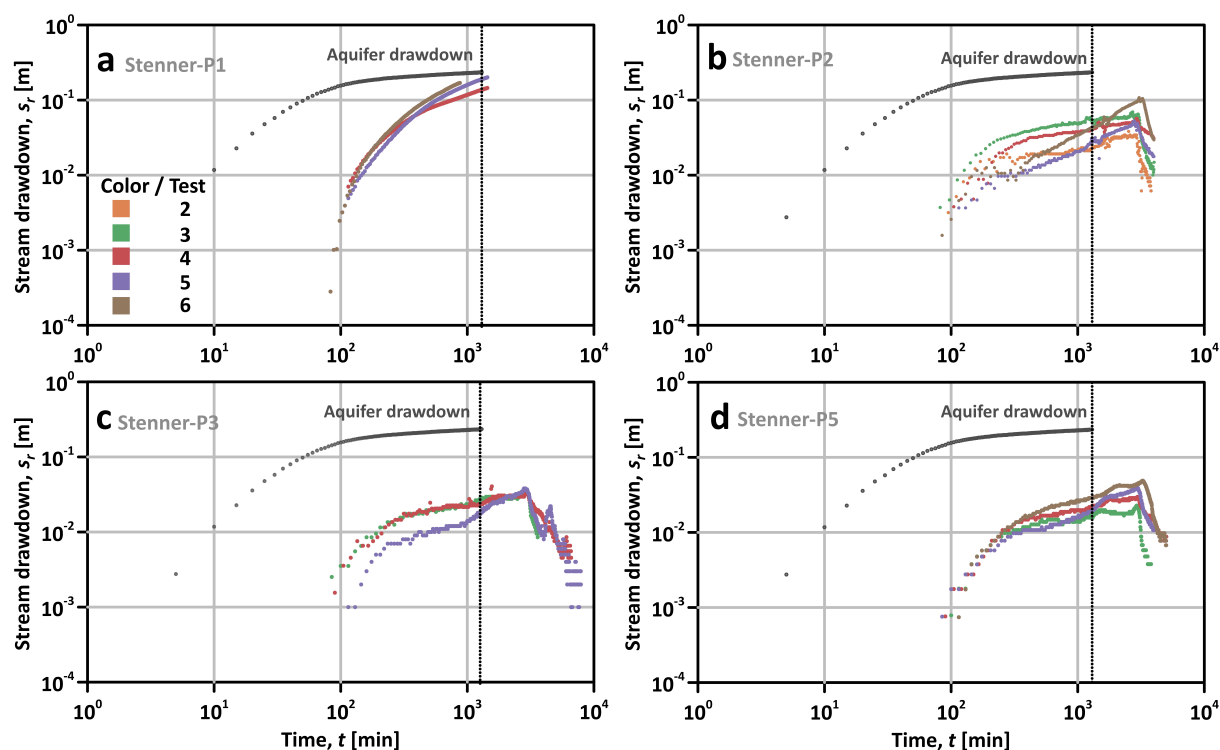
Figure 14. Log-log plots of transient stream stage drawdown response to pumping observed in stream channel stilling wells (a) Stenner-P1, (b) Stenner-P2, (c) Stenner-P3, and (d) Stenner-P5. The data also show stage recovery after pumping (dashed lines for pumping after 48 hrs). Aquifer response (gray dots) is included for comparison.
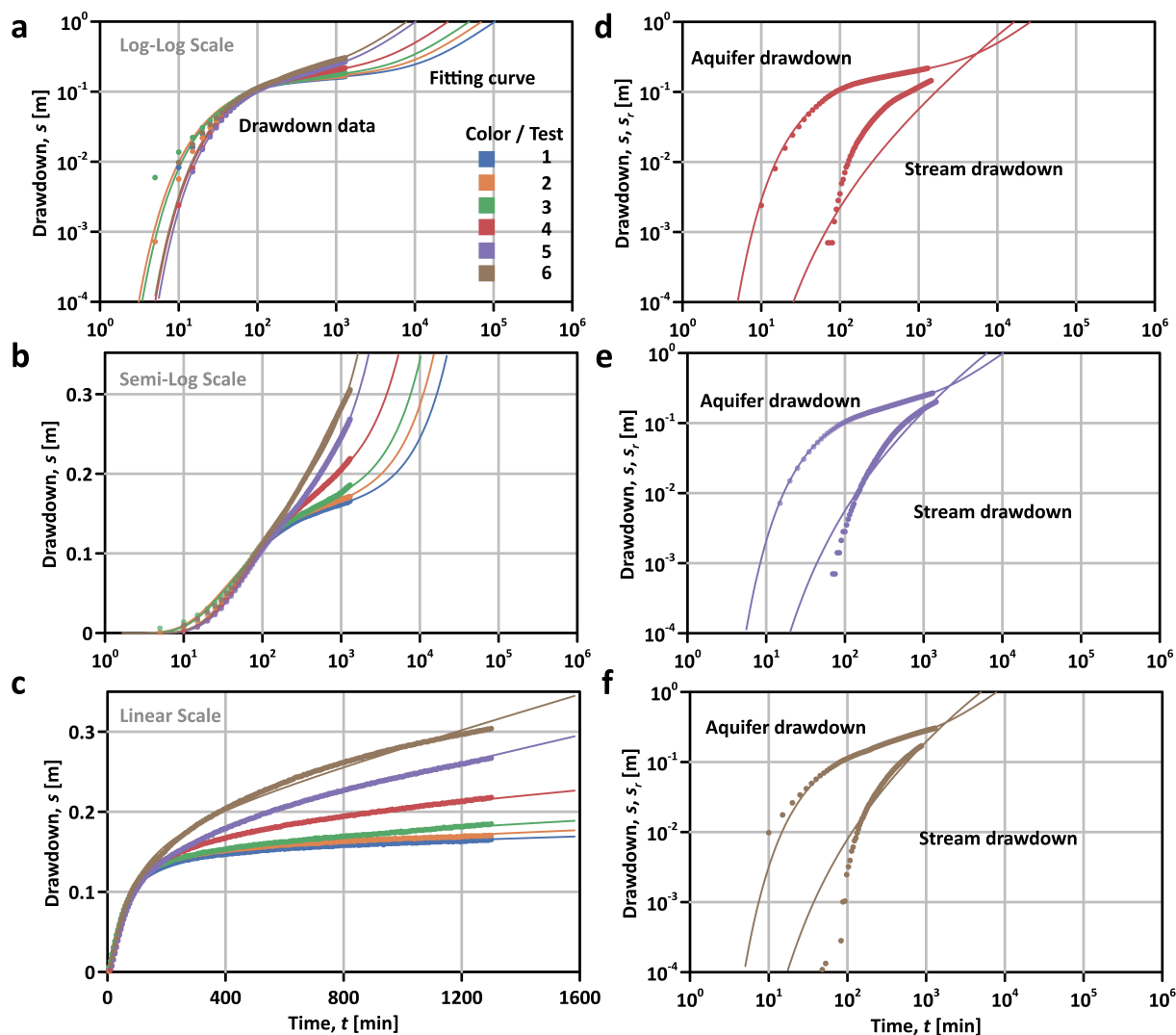
Figure 15. Results of transient analysis of aquifer drawdown response from individual tests showing model fits to observation well data in (a) log-log scale, (b) semi-log scale, and (c) in linear scale. Model predicted stream drawdown response is compared to observations in (d), (e), and (f) using parameters estimated from aquifer data.
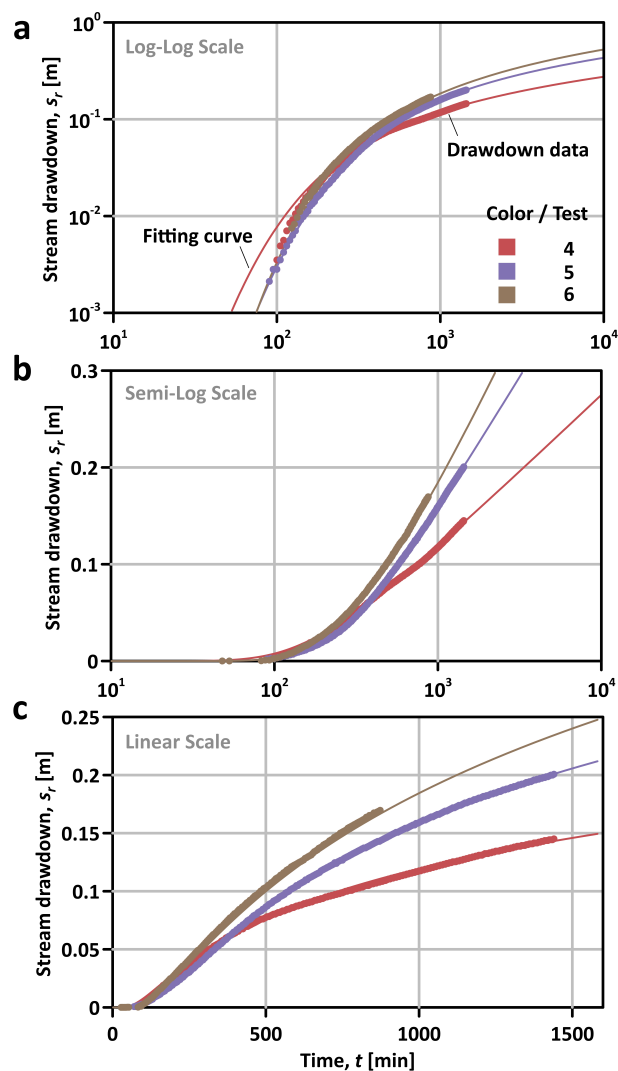
Figure 16. Results of transient analysis of stream drawdown response from individual tests showing model fits to the data for Stenner Creek stilling well S1. The results are plotted on (a) log-log, (b) semi-log, and (c) linear scales.
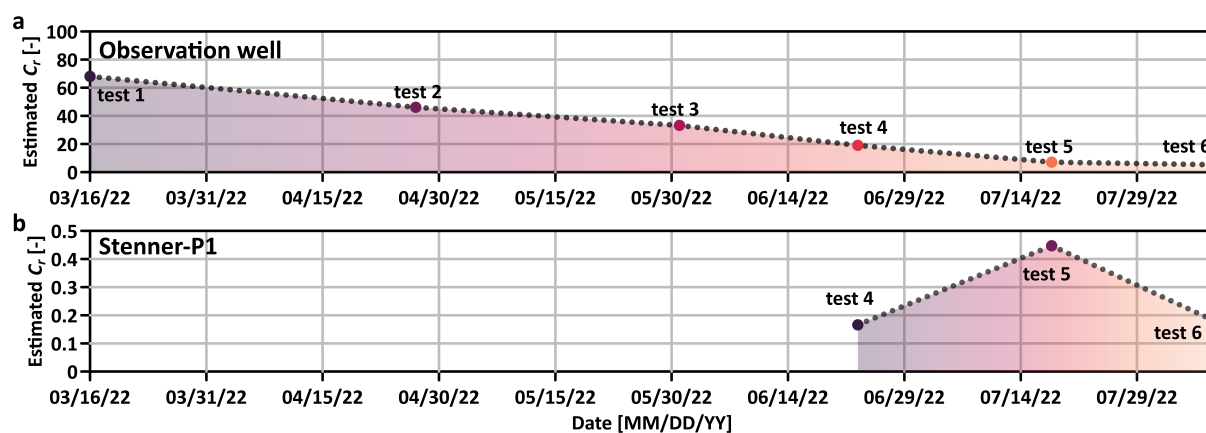
Figure 17. Time series of C_r estimated from the (a) observation well and (b) Stenner-P1 from pumping tests.

Table 1. Definitions of dimensionless variables and parameters based on a characteristic length of $L_c = R$, a characteristic time of $T_c = R^2/\alpha_x$ with $\alpha_x = K_x/S_s$ and a characteristic head of $H_c = Q/(2\pi b K_x)$.

Symbols	Definitions	Symbols	Definitions
$s_{D,i}$	s_i/H_c	κ	K_y/K_x
$s_{D,r}$	s_r/H_c	β_D	$\beta R/K_x$
x_D	x/R	β_D^*	$\beta_D/C_{D,r}$
y_D	y/R	$C_{D,r}$	$C_r/S_s R$
t_D	t/T_c	W_D	W/R
b_D	b/R	q_D	$2\pi b R q/Q$
b_D'	b'/R	$Q_{D,r}$	Q_r/Q

Table 2. Results of parameter estimation using NPS solution for six tests in the observation well.

Test	K_x (m/s)	κ (-)	S_s (1/m)	β (1/s)	C_r (-)
1	8.31×10^{-5}	0.591	1.46×10^{-5}	4.14×10^{-5}	68.0
2	8.31×10^{-5}	0.591	1.46×10^{-5}	4.09×10^{-5}	46.1
3	8.31×10^{-5}	0.674	1.46×10^{-5}	4.02×10^{-5}	33.2
4	8.31×10^{-5}	0.978	1.46×10^{-5}	3.56×10^{-5}	19.0
5	8.31×10^{-5}	1.09	1.46×10^{-5}	3.54×10^{-5}	7.09
6	8.31×10^{-5}	1.08	1.46×10^{-5}	3.49×10^{-5}	5.54
average	8.31×10^{-5}	0.836	1.46×10^{-5}	3.81×10^{-5}	29.8

Table 3. Estimated parameter values using NPS solution for the three recorded tests in the Stenner-P1. Parameters κ and β were fixed to values estimated with aquifer observation well drawdown data.

Test	K_x (m/s)	κ (-)	S_s (1/m)	β (1/s)	C_r (-)
4	8.88×10^{-4}	1.0	6.33×10^{-4}	1.03×10^{-4}	0.166
5	5.14×10^{-4}	1.0	5.19×10^{-4}	1.03×10^{-4}	0.447
6	3.92×10^{-4}	1.0	5.22×10^{-4}	1.03×10^{-4}	0.180